Minerals Engineering 186 (2022) 107743

Contents lists available at ScienceDirect

Minerals Engineering

journal homepage: www.elsevier.com/locate/mineng

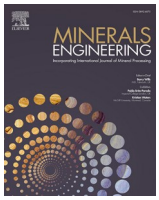

A review of the influence of blast fragmentation on downstream processing of metal ores

Eric Munene Kinyua [a,b,1,*], Zhang Jianhua [a], Richard M. Kasomo [b], Dalmus Mauti [a,b], Jackson Mwangangi [a]

[a] School of Resources and Environmental Engineering, Wuhan University of Technology, Wuhan 430070, China
[b] School of Mines and Engineering, Mining and Mineral Processing Engineering Department, Taita Taveta University, Voi 635-80300, Kenya

ARTICLE INFO

Keywords:
Blast optimization
Comminution
Mineral recovery

ABSTRACT

Rock fragmentation is one of the most commonly optimized blasting outcomes due to its significant influence on the efficiency of downstream operations. This paper reviews the influence of blast fragmentation on processing of metal ores. Two aspects of rock fragmentation that influence downstream mineral processing operations include the particle size of the run-of-mine ore and the degree of internal microfracturing in the fragments induced by blasting. The main influences identified include productivity of comminution equipment, energy consumption in comminution equipment and mineral recovery. An increase in blasting energy results in higher throughput and energy reduction in comminution circuits. Increase in blasting energy results in energy savings in the overall mining operations. However, when increasing the blasting energy, the environmental and safety impacts must be taken into consideration. Blast-induced microfractures increase the permeability of the fragments, therefore enhancing mineral exposure to leaching reagents and consequently may lead to higher mineral recoveries, particularly in heap and dump leaching operations which employ-one-stage comminution. However, the textural characteristics of the ore also influence the mineral recovery. Further research should focus on establishing the relationship between blast intensity and mineral leaching recovery for metal ores of different textural properties.

1. Introduction

In surface mining, excavation and cutting equipment can dig soft weathered ore with high productivity. However, above a certain level of rock hardness and competence, the productivity of excavation equipment is reduced significantly and therefore blasting is required to extract the ore more efficiently (Scott, 2009). Rock blasting in hard rock mining and quarrying is in a sense the first stage in ore comminution that involves the application of pressure generated by explosives to remove ores from their natural beds and reduce the size of the rock mass for easier handling by loading, haulage and comminution equipment (Wills and Finch, 2015; Dunford, n.d.; Shehu et al., 2020). Bench blasting in surface mines involves designing the blast according to the desired outcome, drilling the blastholes, charging the blastholes with explosives, and initiating the explosives. Fig. 1 shows a simple bench blast geometry.

In surface mining, blasting performance may be evaluated in terms of the degree of rock fragmentation, the volume of rock broken, displacement and muckpile profile, damage to the remaining rock, ground vibrations, airblast, flyrock, toxic gases emissions and ore dilution (Bhandari, 1997; Seccatore et al., 2013; McKenzie, 2013). Rock fragmentation is one of the most commonly optimized blasting outcomes due to its significant influence on downstream operations (Grundstrom et al., 2001; Ouchterlony, 2003). The degree of rock fragmentation influences the productivity of excavator and loader, the throughput of crusher and mill, the energy consumption of comminution equipment, and the price of crushed end-products such as the industrial minerals and the construction aggregates (Sanchidrián et al., 2012).

There are two major effects of blasting on fragmentation: (i) size distribution of the muckpile fragments and (ii) creation of microfractures in the fragments (Asgari and Farshad, 2015; Khademian et al., 2017; Shehu and Hashim, 2020; Ouchterlony, 2003). The former effect is seen and can be estimated directly by sieve analysis or image analysis techniques while the latter is unseen with the naked eyes and require

* Corresponding author.
E-mail address: ericinyu@hotmail.com (E.M. Kinyua).
[1] First author.

https://doi.org/10.1016/j.mineng.2022.107743
Received 15 March 2022; Received in revised form 24 June 2022; Accepted 14 July 2022
Available online 20 July 2022

some form of magnification to be quantified. The degree of rock fragmentation in blasting may therefore be evaluated in terms of the particle size distribution of the fragments produced and the degree of micro-fracturing in the fragments (Seccatore, 2019; Workman and Eloranta, 2003; Ouchterlony, 2003).

2. Mine-to-mill blasting

Traditionally, blasting is designed to fracture the in-situ rockmass to prepare it for excavation and subsequent transport without much regard to downstream milling operations (Kanchibotla et al., 1998). Production blasts are designed to achieve optimal shape and swell of the muckpile and optimal particle size distribution primarily for increased shovel and truck productivity in addition to ensuring minimal negative impacts on the environment, dilution and integrity of the pit walls (Janković and Valery, 2002). Also, the mining industries traditionally manage mining operations (drilling, blasting, loading and hauling) and milling operations (crushing, grinding, and metal recovery) separately by adopting extreme control measures on the capital and the operational costs. Cost minimization is attained through achieving production targets at minimum costs in each stage. While this approach may reduce the mining costs, it may not reduce the overall total mining and milling costs (Esen, 2013). This is because all operations in the mining value chain are interdependent and the result of the upstream mining operations have a significant effect on the efficiency of downstream milling operations (Esen, 2013; Grundstrom et al., 2001). The 'mine-to-mill blasting' approach involves identifying the leverage that blast results have on different downstream operations and then optimizing blasting to achieve the results that maximize the overall profitability of the mine rather than the individual operations (Grundstrom et al., 2001).

One of the approaches employed to establish the optimum balance between blasting and downstream operations is the analysis of the unit costs (Fig. 2) where the savings in downstream processes outweigh the increased cost of higher degree of fragmentation in metal mines (Hikita, 2008). Obviously, environmental and safety considerations must be made when designing optimum blasts (Dinis da Gama and Jimeno, 1993). Fig. 3 shows the relationship between the degree of fragmentation (increasing to the right) and the environmental impacts of primary and secondary blasting. At a certain level of fragmentation, the combined environmental effects of primary and secondary blasting are at a minimum. Thus, optimum blasting is governed by not only what level of fragmentation is the most economically desirable, but one which also offers the lowest negative environmental and safety impacts (Hikita, 2008).

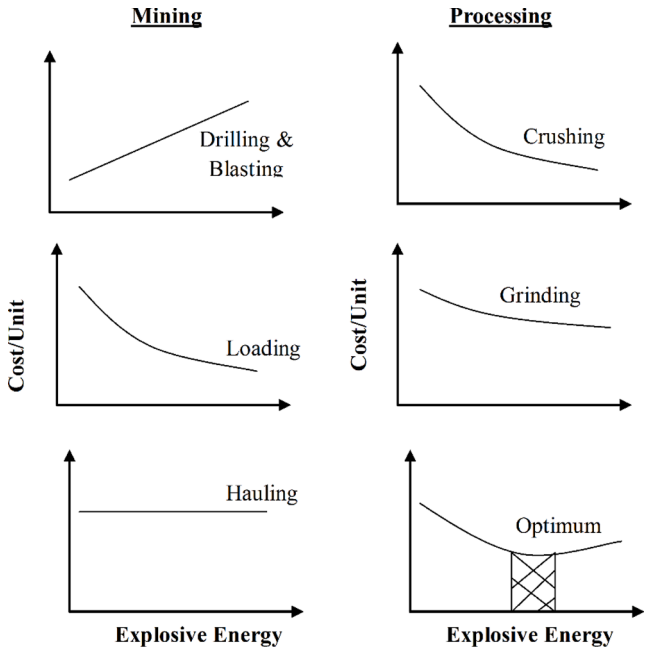

Fig. 2. Relationship between the unit costs of mining operations and the blasting effort (Nielsen and Kristiansen, 2020).

3. Factors influencing rock fragmentation

Rock fragmentation in bench blasting operations depends on the two groups of factors: (i) controllable factors including blast design geometry and explosive properties and (ii) uncontrollable factors which mainly include the rock properties (Lyana et al., 2016; Ayaga, 2016; Singh et al.,

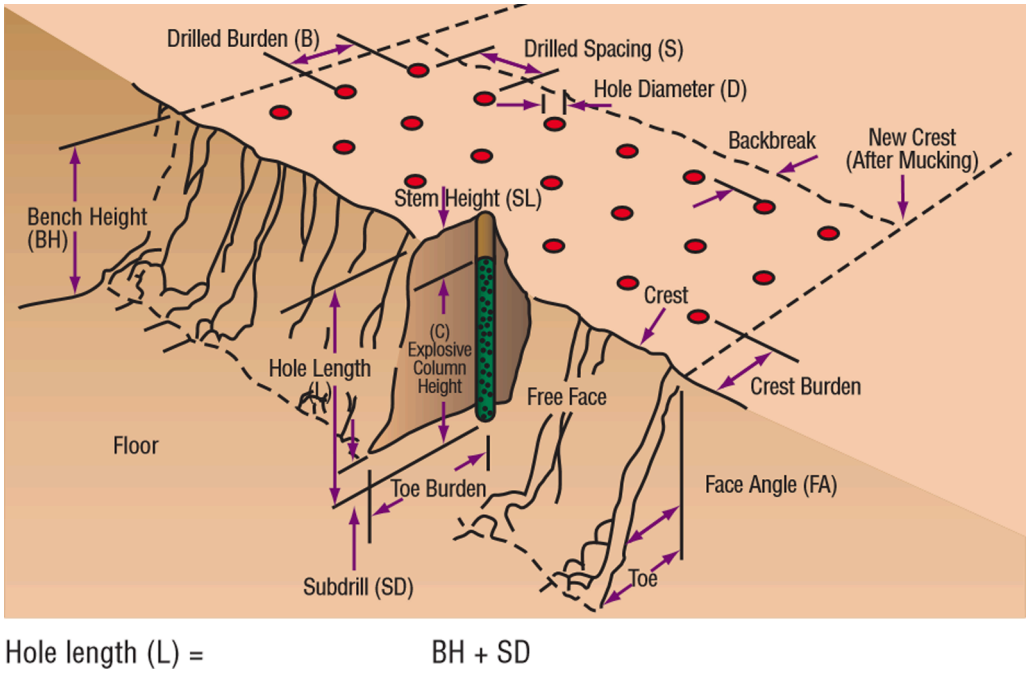

Fig. 1. Pictorial view of bench blast geometry (Nobel, 2010).

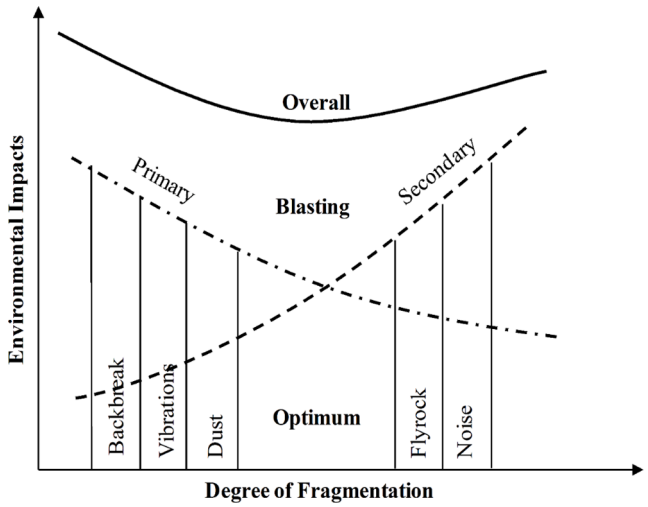

Fig. 3. Relationship between the environmental impacts and the degree of blast fragmentation (Dinis da Gama and Jimeno, 1993).

2016; Shehu and Hashim, 2020) (Fig. 4). Other uncontrollable factors include regulatory constraints such as vibrations, airblast, flyrocks, toxic gases, bench wall stability and the distance to the nearby buildings and other infrastructures (Shehu and Hashim, 2020; Ayaga, 2016). Optimisation of blast fragmentation involves modification of the standard blast design to suit the site conditions of blasting area while ensuring that the environmental regulations related to blasting operations are not violated (Fernández et al., 2022; Müller et al., 2009; Ayaga, 2016). In principle, fragmentation is usually managed by either modifying the blast geometry or by increasing or reducing the specific consumption of explosives. The choice of any approach mainly depends on the relationship between drilling cost, explosive costs and the restrictions imposed (Shehu and Hashim, 2020).

3.1. Controllable factors

The controllable factors that influence rock fragmentation include the burden, spacing, blasthole diameter, stemming, bench height, blasthole length, firing pattern, initiation sequence, delay timing, subdrill length, powder factor, explosive amount per hole, velocity of detonation of explosive, detonation pressure, explosive density, charge density and explosive strength (Mulenga, 2020; Shehu and Hashim, 2020; Ouchterlony, 2003). The most important controllable parameters include spacing to burden ratio, burden to hole diameter ratio, stemming column length, stiffness ratio, firing pattern and delay sequence, powder factor, velocity of detonation, detonation pressure and explosive density (Mulenga, 2020).

3.1.1. Spacing to burden ratio (S/B)

Spacing (S) refers to the distance between adjacent blastholes in a row which controls the mutual charge stress effect between adjacent blastholes (Bhandari, 1997; Olofsson, 1990). In the design of a bench blast, spacing is calculated as a function of burden, hole depth, primer location and the initiation interval (Bhandari, 1997). Burden (B) is the distance from a blasthole in a row to the nearest free space (Olofsson, 1990). There are two types of burden: drilled burden and short burden. The drilled burden is the distance between blasthole rows and the nearest free face measured perpendicular to the blasthole rows while the short burden is the distance between the detonating blastholes and the nearest free face developed during the blast (Agyei and Owusu-Tweneboah, 2019). In a typical bench blasting operation involving multiple rows, the blastholes with lower delay periods detonate and create new faces, and therefore the true or effective burden is dependent on the delay pattern employed (Bhandari, 1997).

The ratio of spacing to burden influences the degree of rock fragmentation. Spacing appreciably less than the burden causes premature splitting between blastholes and early loosening of the stemming, resulting in rapid release of gases to the atmosphere, backbreak and generation of boulders in the muckpile (Bhandari, 1997). When S/B ratio is too high, each blasthole charge fragments and detaches a prismatic section of rock, with the possibility of some section of the rocks midway the blastholes remaining intact; this too results in coarse fragmentation (Bhandari, 1997). There is an optimum S/B ratio suitable for a given bench blasting operation. For most mining operations, S/B of between 1 and 2 is usually employed (Agyei and Owusu-Tweneboah, 2019; Bhandari, 1997). An optimal S/B ratio for staggered pattern is 1.15 and for rectangular pattern is 1.25 (Hagan, 1983).

An increase in S/B results in finer fragmentation up to a certain optimum limit. Singh et al. (2016) in their study of rock fragmentation control in three coal mines found that an increase in S/B ratio resulted in a decrease in the mean fragment size and an increase in the uniformity index of the blasted material and that the optimum fragmentation

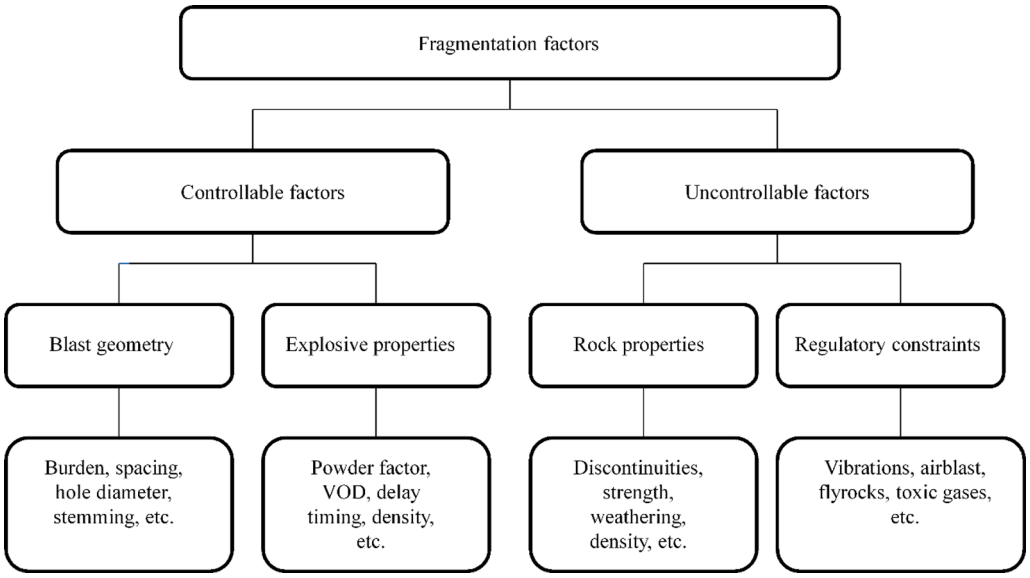

Fig. 4. Factors influencing rock fragmentation in surface bench blasting (Shehu and Hashim, 2020).

results were achieved at S/B of between 1.1 and 1.3. Roy et al. (2016) in their study of rock fragmentation in four iron ore mines established that increasing S/B results in an increase in the uniformity index of the material. Prasad et al. (2017b) in their study on fragmentation of overburden sandstone rock benches found that an increase in S/B in the range of about 1.0 to 1.3 resulted in reduction of the mean fragment size (K50) and maximum fragment size (K80).

3.1.2. Burden to blasthole diameter ratio

The burden affect the entire performance of the blast since the burden dimension is the first step in designing the proper confinement for a blast. If the burden is too large, the rock will not be broken and displaced properly. If the burden is too small, the broken rock will spread across the pit (Konya and Konya, 2019). Increasing the burden to blasthole diameter ratio results in coarser fragmentation. A decrease in burden to blasthole diameter ratio results in finer fragmentation and higher uniformity index of the blasted fragments (Shahrin et al., 2019; Singh et al., 2016).

The choice of the burden to blasthole diameter ratio depends on a combination of several factors including rock characteristics, type of explosive, structural geology of the rock, utilization of the explosives, size of the blasting operation, bench height and the desired fragmentation (Konya and Konya, 2019; Bhandari, 1997). Konya and Konya (2019) recommends burden (in feet) to explosive diameter (in inches) of 24 for ammonium nitrate fuel oil (ANFO) explosive in an average rock and 30 to 36 for emulsion explosives depending on the condition of the rock. Smaller diameter blastholes are suitable in cases where the joints or bedding planes divide the burden into large blocks or where hard boulders lie in the matrix of softer strata; this ensures that each block or boulder has an explosive (Bhandari, 1997).

3.1.3. Stemming column length

Stemming refers to the inert material such as crushed gravel, drill cuttings, sand, clay or water in plastic bags which is inserted in the collar of the blasthole after charging and used to seal the blasthole temporarily in order to confine the gases produced by explosive detonation until they have adequate time to fracture and move the rock (Rustan, 1998; Olofsson, 1990). Adequate stemming also prevent excessive noise, airblast, flyrock, backbreak, and dampens dust and mine fires (Rustan, 1998; Bhandari, 1997). Crushed gravel is the most preferred stemming material due to its high effectiveness compared to other materials. Konya and Konya (2019) recommends stemming to burden ratio of 0.7 when using crushed gravel as the stemming material and 1.0 to 1.2 when using other materials.

The choice of stemming column length is dependent on the type of rock formation to be blasted. When the rockmass has a high frequency of natural cracks and several planes of weaknesses, relatively long stemming columns can be used. When the rock is hard and massive, the stemming should be short to prevent excessive noise, airblast, and backbreak (Bhandari, 1997; Mishra, 2009). The stemming column length varies from 12 times the blasthole diameter in the case of hard competent rock (uniaxial compressive strength $>$ 210 MPa) to 30 times the diameter of blasthole for soft rock (uniaxial compressive strength $<$ 30 MPa) (Pradhan, 1996).

The stemming column is usually-one of the main sources of oversize fragmentation due to the absence of explosives in the column (Ouchterlony, 2003). An increase in stemming length to burden ratio results in coarser fragmentation (Roy et al., 2016; Prasad et al., 2017a; Singh et al., 2016). One way of reducing oversize fragmentation at the stemming region is digging stabholes. Stabholes are short holes drilled to about 75 % of the stemming height between the ordinary blastholes and are charged with a small charge called a stabcharge (Chiappetta, 1998a; Ouchterlony, 2003).

3.1.4. Stiffness ratio

Stiffness ratio is the ratio of bench height of a blast to its burden (Konya and Konya, 2019; Singh et al., 2016). Smaller stiffness ratios results in coarser fragmentation (Roy et al., 2016; Singh et al., 2016). A high stiffness ratio results in easier displacement and deformation of the rockmass and good fragmentation (Rai, 2007; Singh et al., 2016). A stiffness ratio of less than or equal to 1 results in cratering whereby the blast display violent blowout with rock ejected vertically and generation of boulders. At stiffness ratio of 4, the rock is broken under the borehole effect which provides proper deformation and movement of the muckpile and good fragmentation (Konya and Konya, 2019). However, high stiffness ratios may result in blasthole deviation (Konya and Konya, 2019; Singh et al., 2016). Blasthole deviation alters the blast design parameters and results in poor blasting performance including poor fragmentation (Adebayo and Akande, 2015). The optimum stiffness ratio is usually engineered in the field-scale blasts by planning suitable bench heights, burden and firing patterns (Rai and Yang, 2010). In most bench blasting operations, stiffness ratio is usually between 1.5 and 4 (Konya and Konya, 2019).

3.1.5. Firing pattern and delay sequence

In a blast, one of the major requirements is that when the blastholes are fired they should create a free space upon which the subsequent blastholes can break and heave the rock. This is achieved by using the appropriate firing pattern and delay interval between initiations of blastholes. The firing pattern affects effective spacing (S_e) to burden (B_e) ratio and in turn affects rock fragmentation (Rai and Baghel, 2004). The delay pattern determines the detonation sequence of blastholes and thus controls the overall movement and direction of the blasted rock and the resulting fragmentation (Bhandari, 1997). There are several types of firing patterns used in blasting operations including row-to-row or line, diagonal, V-type, chevron, among others (Singh and Cheung, 2017; Rai and Baghel, 2004; Choudhary, 2013). The commonly used delay types include inter-hole surface, inter-row surface and in-hole (Bhandari, 1997).

A good firing pattern and delay sequence ensures sufficient delay time between blasthole charges and between row charges to create space for the blasted rock from the succeeding rows (Olofsson, 1990). The sequentially generated free face with blast progression provides a reflection surface for the shockwave which enhances rock fragmentation (Choudhary, 2013). A short inter-row delay timing causes the burden from the front row to remain in place while the blastholes in the subsequent row are fired resulting in improper relief and excessive confinement. This causes upward cratering that results in poor fragmentation with high and tight muckpiles, large boulders at the collar of the blasthole, backbreaks, and overbreaks (Marton and Crookes, 2000; Rai, 2021; Olofsson, 1990). On the other hand, too long inter-low delay timing results in unwanted spreading of the material as the fragments from the previously fired rows fail to confine the material from subsequently fired rows to prevent excessive throw (Rai, 2021). To achieve good fragmentation, Rai (2021) suggests that for weaker rock formations, longer inter-row delay timing should be employed while for competent rocks, shorter delays should be used. In weaker rock formations, heaving effect is paramount for progressive burden relief and placement while in stronger rocks, shattering effect is crucial during the breakage of the rock. Shattering effect is promoted by in-flight collisions between the broken rock fragments which improve the degree of rock fragmentation (Rai and Baghel, 2004).

3.1.6. Powder factor

Powder factor refers to the amount of explosives (kg) consumed per cubic meter or tonne of the rock blasted (Agyei and Nkrumah, 2021; Ayaga, 2016). The amount of explosive used in a given blasting operation is dependent on the type of explosive, rock properties and the desired fragmentation (Singh and Cheung, 2017). Blasting with higher powder factors results in finer fragmentation (Singh et al., 2016; Prasad et al., 2017a) and higher internal microfracturing of the rock fragments (Workman and Eloranta, 2003; Ouchterlony, 2003). However,

increasing the powder factor beyond a certain level may also cause negative effects such as early ejection of stemming column, overbreak, backbreak, flyrock, ground vibrations and damage to the excavation walls (Agyei and Nkrumah, 2021; Singh and Cheung, 2017; Workman and Eloranta, 2003).

The optimum powder factor can be regarded as the energy available to yield the desired fragmentation without causing negative effects (Singh and Cheung, 2017). Agyei and Nkrumah (2021) reviewed various methods estimating the required powder factor in surface bench and underground blasting operations which include empirical approaches, regression models, artificial neural network models, comminution theory and the Bond's work index. These methods generally focus on the relationship between rock mass properties, property of the explosive, blast geometry and the interaction between specific energy and particle size embodied in the comminution theory.

3.1.7. Velocity of detonation

Velocity of detonation (VOD) is the speed with which detonation wave travels through an explosives column (Bhandari, 1997; Olofsson, 1990). The VOD of an explosive defines the rate of energy release in the rockmass and therefore influences the degree of rock fragmentation (Jimeno et al., 1995). Every explosive has a specific ideal VOD. The actual VOD of an explosive is influenced by several factors including its charge density, chemical composition, blast hole diameter, degree of confinement, initiation (temperature, degree of priming and aging of the explosive), etc. (NIRM, 2001; Ouchterlony, 2003; Kondelchuk and Novikov, 2005). Increase in charge density, blasthole diameter and confinement results in significant increase in VOD of an explosive (Jimeno et al., 1995). Insufficient energy during initiation causes the detonation of explosive to start with a low speed. Aging significantly reduce VOD of an explosive (Kondelchuk and Novikov, 2005). The use of explosives with high VOD results in finer rock fragmentation (Kabwe, 2018; Ouchterlony, 2003). Also using an explosive with a high VOD increases the micro-crack content in the muckpile fragments (Ouchterlony, 2003).

3.1.8. Density of explosive

The density of an explosive refers to the specific weight in kilograms per litre (kg/l) or grams per cubic centimetre (g/cm^3) of an explosive (NIRM, 2001; Olofsson, 1990). The density of an explosive directly influences the charge concentration, detonation velocity and detonation pressure and thus, the rock fragmentation (Kondelchuk and Novikov, 2005; Olofsson, 1990). The greater the density, the more the fragmentation (Jimeno et al., 1995). If the density is very low, the blasting agents become sensitive to the detonating cord, which begins to initiate them before detonation of the primer cartridge. Conversely, if it is very high, the explosive can become insensitive and fail to detonate (Kondelchuk and Novikov, 2005). The linear charge concentration of an explosive (q_l) in a blasthole is related to explosive density and charge diameter as shown in Eq. (1) (Jimeno et al., 1995).

$$q_l = 7.854 \times 10^{-4} \times \rho_e \times D^2 \quad (1)$$

where q_l is the charge concentration in a blasthole (kg/m), ρ_e is the explosive density (g/cm^3) and D is the charge diameter (mm).

The density of an explosive is one of the most important factors considered in calculating the amount of charge required for a blast. A common practice is that in the bottom of the blastholes where more energy concentration is required, higher density explosives such as gelatin or watergels are used whereas lower density explosives such as ANFO and powder based explosives are used in the column charges (Jimeno et al., 1995). Also, depending on the desired fragmentation, the use of high density explosives may permit wide spacing of the blastholes (Olofsson, 1990).

3.1.9. Detonation pressure

Detonation pressure is the pressure associated with the reaction zone of a detonating explosive (Bhandari, 1997). When an explosive detonates, the detonation pressure is released, almost instantaneously, in a shock wave which exists for only a fraction of a second at any given place. Thus, this sudden pressure shatters the rock rather than displacing it and is generally accepted as providing brisance or shattering effect of an explosive. This brisance is dependent upon the suddenness with which the gaseous products of an explosive detonation are liberated (Kondelchuk and Novikov, 2005). Detonation pressure of an explosive is dependent on the density of explosive, detonation velocity and the ingredients which it is composed of (Jimeno et al., 1995; NIRM, 2001). Detonation pressure of an explosive may be estimated by Eq. (2) (Jimeno et al., 1995).

$$PD = 432 \times 10^{-6} \times \rho_e \times \frac{VD^2}{1 + 0.8\rho_e} \quad (2)$$

where PD is the detonation pressure (MPa), ρ_e is the density of explosive (g/cm^3), and VD is the detonation velocity (m/s).

Detonation pressure of an explosive is related to the stress level induced in the material being blasted and therefore influences the fragmentation of the rockmass (Kondelchuk and Novikov, 2005). In hard and competent rocks, fragmentation is more effected with high detonation pressure explosives due to the direct relationship that exists between this parameter and the breakage mechanism of the rock (Kondelchuk and Novikov, 2005).

3.2. Uncontrollable factors

The main uncontrollable factors that influence rock fragmentation are the rockmass properties which may also be referred to as the geological features of the rock (Lyana et al., 2016; Singh et al., 2016); these factors influence the degree of rock fragmentation more than other factors (Hagan, 1995). The rock properties influencing rock fragmentation may be broadly classified into two groups: (i) the intact rock properties and (ii) the structural discontinuities (Mulenga, 2020; Lyana et al., 2016). The intact rock properties include strength, elastic properties, density, porosity, mineral composition, mineral grains, etc. (Mulenga, 2020; Bhandari, 1997). The structural discontinuities include bedding planes, joints, faults, foliations, fracture planes, cleavages, cavities, etc. (Bhandari, 1997). The intact rock properties mainly influence rock fragmentation in competent and massive rockmass (Chiappetta, 1998b) while the structural discontinuities divide the rockmass into separate blocks which can significantly influence the degree of rock fragmentation (Chakraborty et al., 1994; Ouchterlony et al., 1990).

3.2.1. Rock strength

The strength of the rock is the major factor that influences rock blastability (Bhandari, 1997). At constant energy of explosives, an increase in the strength of the rock results in coarser rock fragmentation (Saliu et al., 2013; Bhandari, 1997). Rock strength may be described by parameters such as tensile strength, compressive strength, uniaxial compressive strength (UCS), point load strength and shear strength (Ayaga, 2016). However, UCS is the most commonly used measure of the strength of the rock due to its high accuracy and reliability compared to other strength measures (Saliu et al., 2013). The UCS of the rock is also related to the ease of generating new fractures in the medium (Bhandari, 1997).

The rock blastability is also affected by its brittle index (Sassa, 1974). Brittle index is defined as the ratio of the uniaxial compressive strength to uniaxial tensile strength. Rocks with higher brittle indexes are easier to blast (Bhandari, 1997).

3.2.2. Elastic properties

The elastic properties of a rock depend on the bonding between the mineral particles in the rock. The elastic properties that influence rock fragmentation include Young's modulus, Poisson's ratio, longitudinal wave velocity, etc. (Bhandari, 1997). Young's modulus is the ratio of stress to strain induced in a solid material under a given loading condition (Rustan, 1998). Young's modulus describes the capacity of the rock to resist deformation by tensile forces. It is difficult for explosive gases to fragment the rock if its Young's modulus is very high (Bhandari, 1997). Poisson's ratio is the ratio of lateral strain to the corresponding axial strain for a material subjected to actual loading (Rustan, 1998; Lógó and Vásárhelyi, 2019). Rocks with a low Poisson's ratio fail directly by brittle failure while those having a high Poisson's ratio fail by plastic failure (Bhandari, 1997). Rocks with lower Poisson's ratio generally yield finer fragmentation when blasted (Sassa, 1974). Longitudinal wave velocity is the velocity at which the rock can propagate the compressive waves (Bhandari, 1997). Rocks with high longitudinal wave velocity require explosives with a higher velocity of detonation to achieve fine fragmentation (Hemphill, 1981).

3.2.3. Rock density and porosity

The density of the rock influences blastability of the rock. The rock density indicates the energy needed to deform and displace the rock. The low-density rocks easily undergo deformation and breakage and need low energy explosives to achieve fine fragmentation while denser rocks require explosives with a higher velocity of detonation (Bhandari, 1997). However, porous rocks with lower density absorb energy resulting in poor fragmentation (Bhandari, 1997).

The porosity of rock also affects rock fragmentation. When highly porous rock is blasted, greater dissipation of energy takes place resulting in considerable crushing and production of fines (Bhandari, 1997). Rock fragmentation is also influenced by pore water pressure. Pore water pressure significantly reduces the strength of the rock, resulting in fine fragmentation (Ash, 1968; Obert and Duvall, 1967).

3.2.4. Mineral composition and grain size

The type and grain size of minerals in the rocks affect porosity and strength of the rocks, and hence the rock fragmentation (Bhandari, 1997). Larger mineral grains reduce the strength of the rock (Vutukuri et al., 1974). The strength of the bonding between the mineral grains in most rocks is less than the strength of the mineral grains themselves. Thus, during the rock breakage, fracture occurs at the boundary of the mineral grains. Rocks comprising fine and interlocked mineral grains are difficult to fragment and need higher energy explosives (Bhandari, 1997).

3.2.5. Structural discontinuities

All rock formations are generally inhomogeneous and anisotropic due to the variation in textural and structural features in the rock mass (Bhandari, 1997). The presence of discontinuities in the rock such as bedding planes, joint planes, fault planes, fracture planes, cleavage, foliation, cavities, floaters, etc. influences the rock fragmentation (Aziznejad and Esmaeili, 2015; Bhandari, 1997). They are characterised by their orientation, spacing, number of sets, persistence, aperture and filling material (Brady and Brown, 2006; Mulenga, 2020). The structural discontinuities of the rock have a greater influence on rock fragmentation than the blast geometry and explosive properties (Bhandari, 1997).

The rock discontinuities' direction against the bench face, the spacing, the aperture and the condition of aperture influence the size of the fragments produced (Lyana et al., 2016). Rock formations with horizontal joints when blasted yield uneven fragmentation with overbreak occurring on the sides of the blasts and in the stemming zone (Bhandari, 1997). Rock formations with vertical or dipping joints parallel to the bench face results in uniform fragmentation with the presence of overbreak, less toe problems resulting in a smooth floor and increased throw of the blast which leads to scattered and low muckpile (Bhandari, 1997; Singh et al., 2016). Rock formations with joints perpendicular to the bench face when blasted with the direction of the blastholes parallel to the strike of the joints yields uniform fragmentation (Bhandari, 1997). When designing a blast for highly jointed rock formation, it is important to know the joint orientation in the pit so that either the bench faces can be reoriented or the delay pattern can be arranged in a manner that a favourable direction of the blast is chosen (Lyana et al., 2016; Burkle, 1980; Bhandari, 1997).

The cavities resulting from dissolution of primary rock minerals by groundwater in some mineral deposits reduce blasting efficiency. Where a constant amount of explosive is charged into each blasthole, the presence of cavities in the blastholes may result in excessive charge concentration in the cavity and a corresponding lack of explosive at the upper part of the blasthole, causing uneven fragmentation. Where the blastholes are charged to a constant stemming length, presence of cavities in the blastholes may allow very heavy charge concentration per blasthole resulting in risks of flyrock, overbreak and excessive fragmentation (Bhandari, 1997). The presence of floaters (boulders of relatively higher strength embedded in a much softer rock) that do not contain any charge results in poor fragmentation as the floaters are simply pushed out intact into the muckpile (Bhandari, 1997).

4. Evaluation of rock fragmentation

4.1. Fragment size distribution

The fragment size distribution refers to the statistical representation of the population of the fragment sizes of the blasted rock, the size in this context referring to the mesh size or screen aperture through which particles can pass (Sanchidrián et al., 2012). The fragment size distribution may be described by either the cumulative size distribution curve of the experimentally-determined particle size analysis data obtained through sieving/image analysis of the muckpile or by fragment size distribution models (Dotto and Pourrahimian, 2018; Coello-Velázquez et al., 2019).

4.1.1. Cumulative size distribution curve

In sieve analysis, a known weight of fragments sample is passed through successively finer sieves and the material retained on each sieve is weighed to determine the percentage weight in each size fraction (Wills and Finch, 2015). The cumulative size distribution curve is then plotted with screen (mesh) size x on the x-axis and percentage of material smaller than the particular screen size (mass fraction passing) on the y-axis (Dotto and Pourrahimian, 2018; Ouchterlony, 2003). The cumulative size distribution function (CDF) is the fraction of the material passing a screen with aperture size x, denoted as $P(x)$ (Ouchterlony, 2003). Fig. 5 shows a typical cumulative size distribution curve obtained by sieve analysis. The x_{50} is the median fragment size which is commonly used as a representative measure of fragmentation, P_0 is the percentage of fragments larger than a typical boulder size x_0 which is related to e.g. handling of big blocks by loaders and trucks or the size of the blocks that the primary crusher cannot swallow, and P_F is the percentage of fine material smaller than a typical fines size. P_F is related to the undesired fines produced for materials such as limestone, coal and construction aggregates (Mckee, 2013; Ouchterlony, 2003).

For fragment size distribution determined by image analysis techniques, the particle area or volume is estimated and the cumulative size distribution is the fraction of the total surface area of the image or the estimated volume (Sanchidrián et al., 2012). Fig. 6 shows a typical cumulative size distribution curve of blast fragments obtained by Split-Desktop image analysis system.

4.1.2. Fragment size distribution models

The description of fragment sizes in the form of cumulative size distribution curves requires a series of pairs of values – the mesh size and the fraction of the material passing. Such a large number of data points

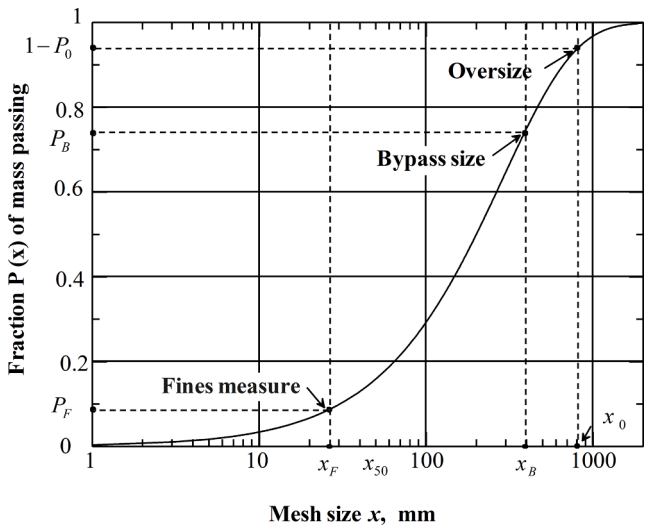

Fig. 5. A typical fragment size distribution curve (Ouchterlony, 2003).

may be substituted by only a few function parameters which can be used to determine any pair of mesh size/fraction passing values. The fragment size distribution models give these function parameters. Blast fragmentation models provide predictions for the parameters of a certain size distribution function (based on the blast design data) from which the whole cumulative size distribution curve can be built (Sanchidrián et al., 2012).

The distributions that describe the size of granular material such as the muckpile fragments are usually expressed in the form of cumulative distribution functions, *P(x)*, which gives the probability that a fragment is smaller than the variable × (Sanchidrián et al., 2012; Ouchterlony, 2003). The most popular distribution function used to describe particle size of the blasted fragments is the Rosin-Rammler function also known as Weibull equation (Rosin, 1933; Sanchidrián et al., 2012; Vesilind, 1980). A recently developed Swebrec function is a modification of the Rosin-Rammler function which better estimates the coarse and fine zones of the distribution (Hüdaverdi and Akyildiz, 2020; Ouchterlony and Sanchidrián, 2019; Ouchterlony, 2005b; Ouchterlony, 2005a). Other fragment size distribution functions include Gilvarry (Gilvarry and Bergstrom, 1961; Gilvarry, 1961), Grady Function (Grady, 1990; Grady and Kipp, 1985), Lognormal (Sanchidrián et al., 2012), Gates-Gaudin-Schumann (Sanchidrián et al., 2012; Wills and Finch, 2015), Log-logistic (Maiti and Kayal, 2020; Sanchidrián et al., 2014), Sigmoidal (Blair, 2004), among others. These distribution functions exist in the form of plain-single (unimodal), rescaled and bimodal components and their different forms have varying capabilities of approximating the sieved fragment data (Blair, 2004; Sanchidrián et al., 2009; Sanchidrián et al., 2012; Sanchidrián et al., 2014).

Rosin-Rammler (RR) is a two-parameter (x_c and n) distribution whose cumulative distribution function $P(x)$ is:

$$P(x) = 1 - exp\left[-\left(\frac{x}{x_c}\right)^n \right], 0 \le x \le \infty \quad (3)$$

where x_c is the scale parameter (characteristic particle size) defined as the size at which 63.2 % $(1 - 1/e = 0.632)$ of the material passes and n is the material uniformity parameter. In the second form of the equation (with base 2), the scale parameter is the median size, x_{50}. The Rosin-Rammler distribution is widely used in blast fragmentation models to predict the parameters of the function from the blast design data (Sanchidrián et al., 2012).

The Swebrec function©(SWE) is an improvement of the Rosin-Rammler's poor predictive capacity in the fines range and coarse range of the fragmentation distribution (Sanchidrián et al., 2012; Ouchterlony, 2005a). The Swebrec function gives good-to-excellent fits to different kinds of sieved fragmentation data with a correlation coefficient > 0.995 over a wide range of fragmentation sizes (Ouchterlony, 2005a). The function has three parameters (x_{max}, x_{50} and b) (Coello-Velázquez et al., 2019; Ouchterlony, 2005a; Ouchterlony and Sanchidrián, 2019).

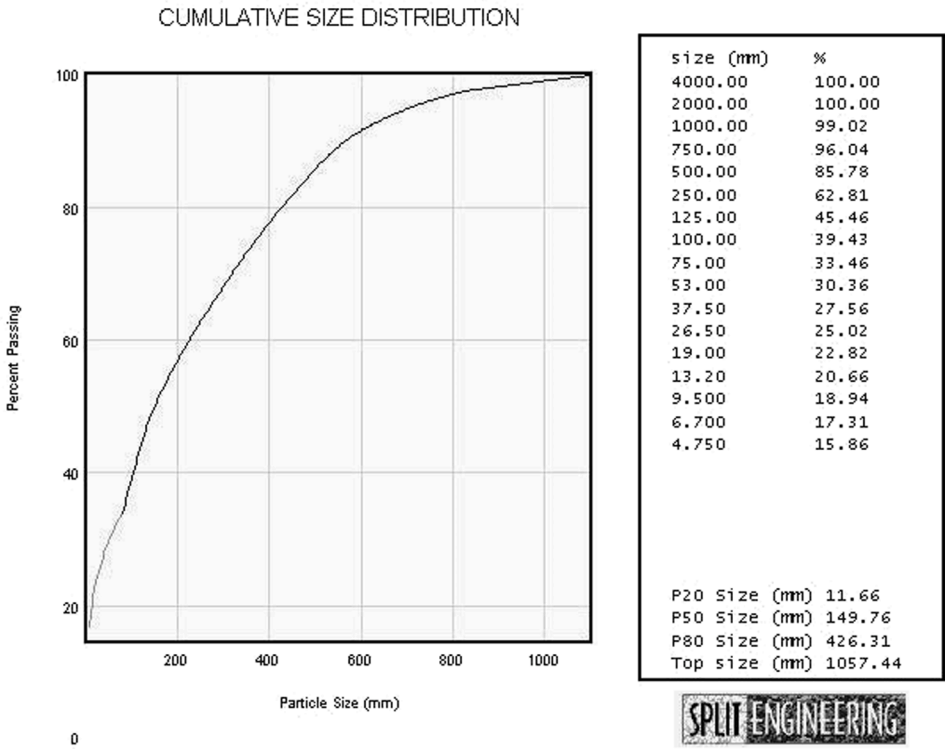

Fig. 6. A typical fragmentation curve by the Split-Desktop system (Siddiqui, 2009).

$$P(x) = \frac{1}{1 + \left[\frac{ln\left(\frac{x_{max}}{x}\right)}{ln\left(\frac{x_{max}}{x_{50}}\right)}\right]^{b}}, 0 < x \leq x_{max} \quad (4)$$

Whereby x_{max} is the maximum size of particles (for which $P = 1$), x_{50} is the sieve size that retains 50 % of the material and b is the shape parameter also known as curve undulation parameter, similar to n in the Rosin-Rammler equation, given by Eq. (5).

$$b = \left[2ln2ln\left(\frac{x_{max}}{x_{50}}\right)\right]n \quad (5)$$

The Gilvarry's function which may be abbreviated GIL was originally used to describe single fragmentation of brittle solids whereby it was determined both theoretically and experimentally that for single fracture of brittle material, the fragment size distribution function of the resulting fragments is based on Griffith's theory of brittle strength (Gilvarry and Bergstrom, 1961; Gilvarry, 1961). The GIL function was thereafter applied to describe the fragmentation statistics under high-velocity impact loading (Sil'vestrov, 2004b) and statistical description of fragmentation of solids under dynamic loading (Sil'vestrov, 2004a). The GIL function is a three-parameter distribution function whose CDF is given by Eq. (6) (Sanchidrián et al., 2012; Sanchidrián et al., 2009).

$$P(x) = 1 - exp\left\{-\left[\left(\frac{x}{x_1}\right) + \left(\frac{x}{x_2}\right)^2 + \left(\frac{x}{x_3}\right)^3\right]\right\}, 0 \leq x \leq \infty \quad (6)$$

where x_1, x_2 and x_3 are related to the densities of cracks of linear, planar and volume type respectively.

The Grady's function describes the distribution of particle sizes produced in dynamic fragmentation processes (Grady and Kipp, 1985; Grady, 1990). The distribution function which can be abbreviated GRA is a power exponential expression and its CDF is written as:

$$P(x) = 1 - \left[1 + \left(\frac{x}{x_g}\right)^{\alpha}\right] exp\left[-\left(\frac{x}{x_g}\right)^{\alpha}\right], 0 \leq x \leq \infty \quad (7)$$

Whereby x_g and α are scale and shape parameters similar to x_c and n of the Rosin-Rammler function.

The lognormal distribution is expressed as (Sanchidrián et al., 2014):

$$F_{LGN(x,x_m,s)} = \frac{1}{s\sqrt{2\pi}} \int_0^x \frac{1}{t} exp\left[-(lnt - x_m)^2/2s^2\right] dt, 0 \leq x \leq \infty \quad (8)$$

where x_m and s are the mean and the standard deviation of the natural logarithm of x respectively.

Log-logistic (LGL) CDF is expressed as:

$$P(x) = \frac{1}{1 + (x/x_{50})^{-\gamma}}, 0 \leq x < \infty \quad (9)$$

where x_{50} is the median size and γ is the scale parameter (Sanchidrián et al., 2014).

The Gates-Gaudin-Schuhmann (GGS) distribution (Gaudin, 1926; Gates, 1915; Schuhmann Jr, 1940) is a power function commonly used in comminution for non-uniform fragment size distribution (Ouchterlony and Sanchidrián, 2019; Wills and Finch, 2015). In the GGS distribution, the cumulative percent passing data is plotted against sieve aperture on log–log axes, leading to a linear trend from which data can be interpolated easily (Wills and Finch, 2015). The linear trend is fitted to the following CDF (Ouchterlony and Sanchidrián, 2019):

$$P(x) = ax^n = \left(\frac{x}{x_{100}}\right)^n = 0.5\left(\frac{x}{x_{50}}\right)^n \quad (10)$$

where $x_{100} = x_{max}$ denotes the size of the largest fragment, x_{50} is the median fragment size, a is a normalization parameter, and n is the uniformity index.

Re-scaling the distribution functions generally reduces the unexplained variance by a factor of about four with respect to the plain function while bimodal components further reduce this unexplained variance by a factor of about two to three (Sanchidrián et al., 2014). Therefore, the re-scaled and bi-components better predicts the size distribution of fragments than their plain-single versions (Sanchidrián et al., 2014; Sanchidrián et al., 2012; Sanchidrián et al., 2009; Blair, 2004).

The Rosin-Rammler, Gilvarry, Grady, log-normal and log-logistic cumulative distribution functions which reach the unity value only at infinite size may be transformed by scaling the abscissa with a maximum size x_{max} and forcing an infinite value of the variable at that point, thereby bringing the function value to unity. This rescaling is accomplished by substituting ξ for x (Sanchidrián et al., 2014) as shown in Eq. (11).

$$\xi = \frac{(x/x_{max})}{1 - (x/x_{max})} = \frac{x}{x_{max} - x} 0 \leq x \leq x_{max} \quad (11)$$

The function, $F_T(\xi)$, with a semi-infinite $(0 \leq \xi < \infty)$ domain, is thus transformed into a finite x domain $(0 \leq x \leq x_{max})$.

For example, the RR function is rescaled as:

$$F_{RR(x,x_c,n)} = 1 - exp\left[-\left(\frac{\xi}{\xi_c}\right)^n\right] = 1 - exp\left\{-\left[\frac{x(x_{max} - x_c)}{x_c(x_{max} - x)}\right]^n\right\}, 0 \leq x \leq x_{max} \quad (12)$$

In the case of SWE function, the rescaled function has no semi-infinite counterpart (Sanchidrián et al., 2014) and is expressed as:

$$F_{SWE(x,x_{max},x_{50},b)} = \frac{1}{1 + \left[\frac{log\left(\frac{x_{max}}{x}\right)}{log\left(\frac{x_{max}}{x_{50}}\right)}\right]^{b}}, 0 \leq x \leq x_{max} \quad (13)$$

Bimodal components of the distribution functions are formed as a linear combination of two unimodal distributions by the following expression (Sanchidrián et al., 2012; Sanchidrián et al., 2014; Sanchidrián et al., 2009):

$$F_{Bi(x,\pi_1,\pi_2)} = (1 - f)F(x, \pi_1) + fF(x, \pi_2), 0 \leq x \leq \infty \quad (14)$$

F is any of the single-component function; π is the vector of the function parameters e.g. (x_c, n) for Weibull, (x_g, α) for Grady and (x_1, x_2, x_3) for Gilvarry. $f(0 \leq f \leq 1)$ is the fraction of the modality with a parameter set π_2 and $1 - f$ is the fraction of the modality π_1. For example, the bimodal component of log-logistic function is:

$$F_{BiLGL} = (1 - f)F_{LGL} + fF_{LGL} = (1 - f)\frac{1}{1 + (x/x_{50,1})^{-\gamma_1}} + f\frac{1}{1 + (x/x_{50,2})^{-\gamma_2}} 0 \leq x < \infty \quad (15)$$

For Swebrec function, no such bimodal component has been established, but an extended version (ExSWE) similar to bimodal component exists to serve a similar purpose (Sanchidrián et al., 2012; Sanchidrián et al., 2014; Ouchterlony, 2005a; Sanchidrián et al., 2009):

$$= \left\{1 + a\left[\frac{ln(x_{max}/x)}{ln(x_{max}/x_{50})}\right]^b + (1 - a)\left[\frac{(x_{max}/x) - 1}{(x_{max}/x_{50}) - 1}\right]^c\right\}^{-1}, 0 < x \leq x_{max}F_{ExSWE(x,x_{max},x_{50},b,a,c)} \quad (16)$$

4.1.3. Measuring particle size distribution

The particle size distribution of the muckpile fragments may be assessed by several methods which can be broadly classified into two groups: direct and indirect methods (Fig. 7) (Siddiqui, 2009; Elahi and Hosseini, 2017; Shehu and Hashim, 2020). Direct methods include screening (sieve analysis), boulder counting and direct measurement of

the rock fragments. Screening is currently the most commonly employed direct technique (Shehu and Hashim, 2020). The indirect methods include observational, empirical models and image analysis techniques (Elahi and Hosseini, 2017; Siddiqui, 2009; Shehu et al., 2020; Tungol et al., 2019; Shehu and Hashim, 2020).

Sieve analysis involves screening rock fragments using sieves of different mesh numbers for different fragment sizes and grouping the fragments according to their sizes (Shehu and Hashim, 2020). Sieving is considered the most precise method of evaluating particle size distribution of fragments but is not commonly used for routine purposes in large scale production blasting operations because it is too costly and time-consuming (Siddiqui, 2009; Cho et al., 2003; Dotto and Pourrahimian, 2018). The method is commonly used for assessing the accuracy of the image analysis techniques and for small-scale production blasts (Cho et al., 2003; Shehu and Hashim, 2020).

The digging and loading rate technique involves assessing the digging and loading rate of a shovel or excavator for a specific muck pile. The technique is based on assumption that the digging and loading rate increases with better (finer) fragmentation (Shehu and Hashim, 2020). The method is not very accurate since the digging rate is not only affected by fragmentation but is influenced by other factors such as truck availability, technical faults with the equipment, operator skills, and other factors. The method may be used for rough comparison of the size distribution of different muck piles (Shehu and Hashim, 2020).

Visual analysis involves a blasting engineer or other expert viewing the blasted muckpile immediately after blasting and giving a subjective opinion on the fragmentation (Sereshki et al., 2016; Mohamed et al., 2019). The technique is quick and simple but of low accuracy because only the apparent surface of the muck pile is assessed and only a very large difference in fragmentation between the two blasts can be noticed (Shehu and Hashim, 2020). The technique is widely used by blasting engineers to arrive at approximations of fragmentation of the muckpile (Sereshki et al., 2016).

Empirical models employ blast design parameters including rock mass factors, blast geometry and explosive factors to predict the size distribution of the fragments. The models are used to predict the cumulative size distribution $P(x)$, mean fragment size x_{50}, particular characteristic size x_c, uniformity coefficient n and other parameters of the fragment size distribution functions (Hüdaverdi and Akyildiz, 2020; Vamshidhar and Venkatesh, 2010). Several blast fragmentation models have been developed to date, Table 1 shows some of these models. The Kuz-Ram model is the most commonly used (Vamshidhar and Venkatesh, 2010; Gheibie et al., 2009; Cunningham, 2005; Ouchterlony, 2003) due to its simplicity in terms of the ease of obtaining the input data and its direct linkage with blast design and rock fragmentation results (Cunningham, 2005). However, the Kuz-Ram model has some drawbacks among them including poor prediction of the fines range and lack of prediction of the effect of timing on fragmentation (Gheibie et al., 2009; Ouchterlony, 2005a; Vamshidhar and Venkatesh, 2010). Some of the recently developed models are an improvement of the Kuz-Ram's inability to accurately predict fragment size distribution, including the Modified Kuz-Ram model (Gheibie et al., 2009), Kuznetsov-Cunningham-Ouchterlony (KCO) Model (Ouchterlony, 2005a), Crush Zone Model (CZM) (Thornton et al., 2001; Kanchibotla et al., 1999) and the Two-Component Model (TCM) (Djordjevic, 1999).

Digital image processing is the second most reliable method after sieving involving the use of computer programs to analyse the fragmentation images acquired through a digital camera, individual frame capture from video or scanned (digitized) photographs (Mohamed et al., 2019; Siddiqui, 2009). The fragment images acquired from muckpile, haul truck, leach pile, draw point, waste dump, stockpile, and conveyor belt are delineated automatically using digital image processing software and the size distribution of the fragments is determined (Mohamed et al., 2019). Examples of the digital image processing systems used include Split-Desktop, BlastFrag, WipFrag, GoldSize, FragScan, TUCIPS, CIAS, PowerSieve, IPACS, KTH and WIEP (Elahi and Hosseini, 2017;

Table 1
Blast fragmentation prediction models.

Fragmentation model	References
Bergmann, Riggle and Wu (BRW) model	Bergmann et al. (1973)
SveDeFo equations	Holmberg (1974); Larsson (1974)
Da Gama model	Da Gama (1983)
Kuz-Ram models	Cunningham (1983); Cunningham (1987); Cunningham (2005)
Kou-Rustan's equation (Saroblast)	KOULLI and Rustan (1993)
Energy Block Transition (EBT) model	Lu and Latham (1998)
Chung and Katsabanis (CK) model	Chung and Katsabanis (2000)
JKMRC models (Crush Zone Model (CZM) and Two-Component Model (TCM))	Djordjevic (1999); Kanchibotla et al. (1999); Thornton et al. (2001)
Kuznetsov-Cunningham-Ouchterlony (KCO) model	Ouchterlony (2005a)
Modified Kuz-Ram	Gheibie et al. (2009)

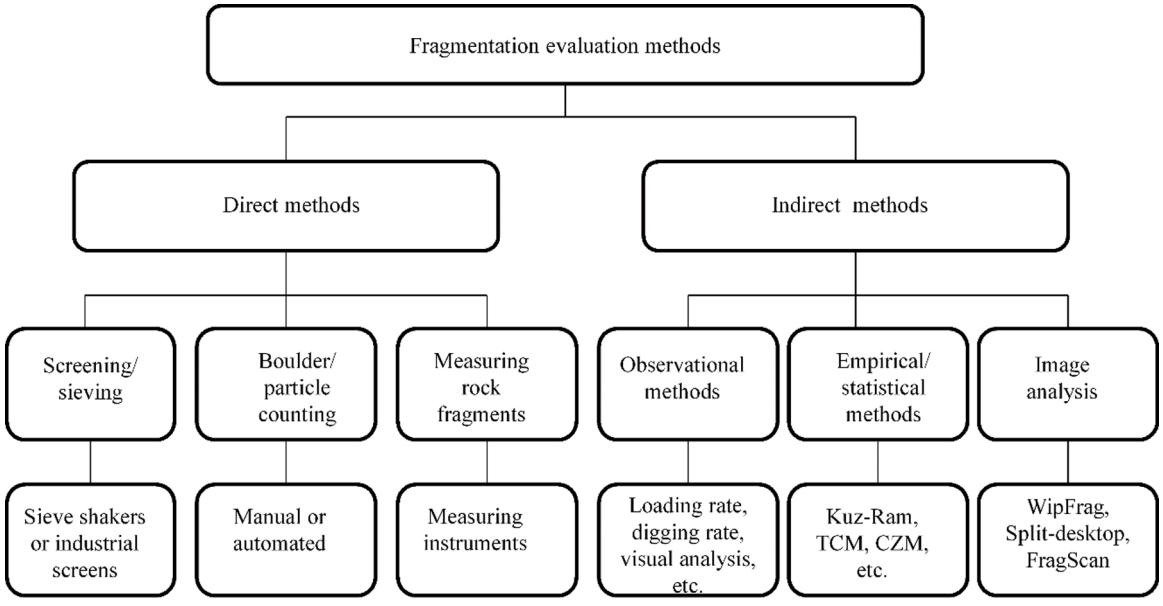

Fig. 7. Methods of measuring particle size distribution (Shehu and Hashim, 2020).

Siddiqui, 2009; Shehu et al., 2020; Shehu and Hashim, 2020). Split-Desktop, WipFrag, FragScan and GoldSize are the most commonly used software packages for determination fragment size distribution (Sereshki et al., 2016; Shehu and Hashim, 2020).

Digital image analysis allows rapid assessment of size distribution continuously without interrupting the production cycle, has no limitation on the size of the sample that can be analysed, and the price of the equipment and the software is relatively inexpensive (Elahi and Hosseini, 2017; Siddiqui, 2009). The techniques are a result of technological advancement and are progressively becoming popular in blast fragmentation measurement (Shehu and Hashim, 2020; Siddiqui, 2009). However, despite their growing popularity, the techniques are prone to errors with accuracy ranging from 2 to 20 % (Siddiqui, 2009). Their inherent errors are mainly associated with image acquisition including underestimation of fines, tilting error, non-uniform lighting, irregular focusing, uneven shutter speed, zooming, edge detection, error in the conversion of 2D to 3D images, sampling error, etc. (Siddiqui, 2009; Cho et al., 2003; Shehu and Hashim, 2020). The currently available digital image analysis systems cannot analyse particles smaller than the size determined by the pixel resolution and it is difficult to obtain a good representative sample for the analysis (Dotto and Pourrahimian, 2018). Their errors can be minimized by capturing high-quality images of a large number of samples for the analysis (Shehu et al., 2020).

4.2. Blast-induced microfracturing

4.2.1. Description of microfractures

Galvez (2011) differentiates two forms of invisible fractures in rock fragments depending on what caused them; these include microcracks and microfractures. Microcracks are naturally generated by rock formation and geological processes such as earthquakes, volcanic eruption and thermal contractions while microfractures are induced by mining-related processes including blasting, crushing and grinding. However, the terms microcracks, microfractures and cracks are sometimes used synonymously. In terms of the size, blast-induced fractures may be categorised into two, namely macrofractures and microfractures (Ouchterlony, 2003; Anders et al., 2014; Parra et al., 2015; Khademian et al., 2017). Macrofractures are visible by the naked eye and range from mm to cm in size (Parra et al., 2015). Microfractures are only visible under magnification and are usually < 1 mm in length and < 0.1 mm in width (Anders et al., 2014). Blast-induced microfractures may be categorised into three types depending on the nature of fracture propagation. These include intergranular fractures formed along mineral grain boundaries, transgranular fractures that cut across multiple mineral grains and intragranular fractures that are generated inside the mineral grains (Akesson et al., 2004). The creation of microfractures in the rock fragments by blasting which results in alteration of the physical properties of the rock is termed as fragment conditioning (Parra et al., 2015).

4.2.2. Theory of formation of microfractures in rocks

The theory formation of cracks or fractures in rocks may be derived from the Griffith theory of brittle fracture (Griffith, 1920). A crack is mathematically assumed to be a sharp slit embedded within an elastic medium (Anders et al., 2014). There are three modes of cracking, namely, Mode I, Mode II and Mode III. Mode I cracks is the opening mode also known as tensile cracks, while Mode II and III are the shear modes. In the formation of tensile cracks (Mode I), the maximum opening between the crack walls, D_{max}, is related to crack length L as shown in Eq. (17) (Anders et al., 2014).

$$D_{max} = \Delta\sigma \frac{(I-v)}{\mu} L \tag{17}$$

where $\Delta\sigma$ is the effective driving stress, v is Poisson's ratio, and μ is the rigidity. The effective driving stress given by $\Delta\sigma = (\sigma_n - p)$ is the difference between the applied stress normal to the crack wall and the pore pressure within the crack.

The stresses near the tip of the crack are expressed as:

$$\sigma_{ij} = K(2\pi r)^{-1/2} f_{ij}(\theta) \tag{18}$$

where r is the distance from the crack tip, K is the stress-intensity factor, and $f_{ij}(\theta)$ are functions that describe the dependence of each stress component on the angle θ from the plane of the crack.

The stress intensity factor for an isolated crack is:

$$K = \Delta\sigma \left(\frac{\pi L}{2}\right)^{1/2} \tag{19}$$

According to Griffith (1920), the crack propagates when the energy released in propagating the crack is just sufficient to create new crack increment. Thus, the crack propagates when K reaches a critical value K_c defined by when the energy release rate G reaches a critical value G_c equal to the surface energy increment which is sufficient to break the bonds at the crack tip (Anders et al., 2014),

$$G_c = \frac{K_c^2}{2(1+v)\mu} = 2\alpha \tag{20}$$

where α is the specific surface energy of the material.

During the crack propagation, $K = k_c$, a constant. According to Eq. (19), the driving stress decreases as the crack length increases (the crack weakens as it lengthens). The crack will thus be unstable when constant stress boundary conditions are reached (Anders et al., 2014). According to the Griffith Energy balance, this instability occurs when the crack attains a critical length L_c expressed as:

$$L_c = \frac{8\mu(1+v)\alpha}{\pi T^2} \tag{21}$$

where T is the tensile strength of the rock. Under constant stress boundary conditions assumed by Griffith, a crack propagates without limit when it reaches this critical length.

When Eq. (17) and Eq. (19) are combined, we obtain.

$$D_{max} = \frac{(I-v)}{\left(\sqrt{\pi/2}\right)\mu} K_c L^{1/2} \tag{22}$$

Eq. (22) predicts that D_{max} scales as $\sqrt{L}$. Fracture will therefore occur when the longest, most favourably oriented crack becomes critical (Anders et al., 2014).

4.2.3. Mechanism of blast-induced microfracturing

The mechanism by which rock fragments and micro-fractures are created by blasting is complex and not yet fully understood (Khademian et al., 2017). The most popular theory is that upon detonation of explosives in the blast hole, the rock breakage occurs in two stages. Firstly, the shockwaves travel outward from the blasthole causing radial cracks to form around the blasthole, then the gases penetrate the cracks which widen them and makes them longer (Olsson et al., 2002; Khademian et al., 2017). The shockwaves are primarily responsible for the generation of microfractures while the gases are responsible for moving/heaving of the rock fragments (Olsson et al., 2002).

The shockwaves may be classified into two types which include the primary compressive waves (P-waves) and the secondary shear waves (S-waves). The P-waves cause transient deformations in the rock mass, part of which are tensile deformations which may open up existing cracks or form new fractures depending on the stress levels (Fig. 8). The negative sign in Fig. 8 is compression while the positive sign is tension. At low-stress levels, the P-waves open up existing cracks in the rockmass. As the stress levels exceed the dynamic tensile strength of the intact rock, the P-waves generate two sets of new fractures. One set is the radial fractures created by tangential tensile stress at the front of the wave while the other set is concentric fractures around the blasthole caused by

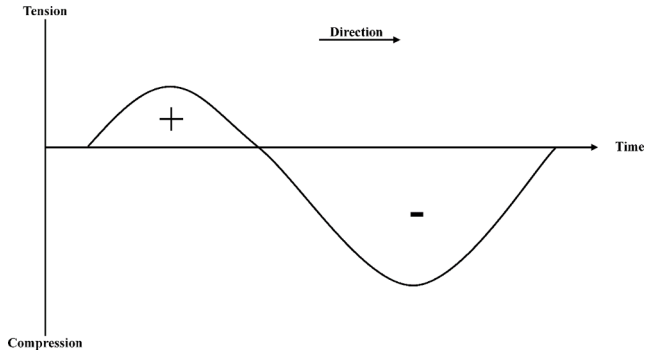

Fig. 8. Compressive (front, negative) and tensile (tail, positive) of the P-wave (Nielsen and Malvik, 1999).

the tensile tail of the wave (Fig. 9). The P-waves are followed by the slower S-waves caused by deformation of the blasthole during explosive detonation. The S-waves may enlarge the fractures earlier created by the P-waves or can also create new ones (Nielsen and Malvik, 1999).

4.2.4. *Estimation of fracture zone around blasthole*

When an explosive charge is fired in the blasthole, first the blasthole is expanded. Then, the shockwave generated creates two damage zones around the blasthole, namely, the crushed and the cracked zones (Fig. 10) (Shadabfar et al., 2020). The crushed zone is formed around the blasthole due to the increase in discontinuities and growth of fine cracks (Wang et al., 2012). The cracked zone is formed more by the blasting shockwaves which radially penetrate the rockmass beyond the crushed zone to the surrounding environment (Saharan et al., 2006; Banadaki and Mohanty, 2012). Beyond the crushed zone and the cracked zone, the explosion effects are observed in the form of ground vibrations (Adhikari et al., 2004; Chi et al., 2019). It then follows that while in the vicinity of the blasthole the excess energy results in crushing and powdering of the rockmass; however, beyond a certain distance from the crushed zone, the energy may be just enough for cracks to propagate along the weak zones with fewer microfractures being formed.

The size of damage zones in the rockmass is a function of input parameters which include rock properties and explosive characteristics (Shadabfar et al., 2020). Consequently, the desired fragmentation (damage) can be achieved through blast design optimization. The optimal values of target parameters may be achieved either by trial-and-error process or mathematically by optimization algorithm (Asl et al., 2018; Leng et al., 2020). Various researchers have proposed different approaches of approximating the damage zones in the rockmass. The approaches may be broadly classified into three groups which include analytical, numerical and experimental (Wei et al., 2009; Yang et al., 2016; Hu et al., 2018; Sun and Sun, 2012). These methods are comprehensively reviewed by Shadabfar et al. (2020). In general, the size of damage zone may be expressed as (Shadabfar et al., 2020):

$$r = f(\theta_1, \theta_2, \cdots \theta_n) \tag{23}$$

where r represent the damage zone radius and θ_1 to θ_n input parameters (rock and explosive characteristics). The most important input parameters are outlined in Table 2.

In analytical methods, a parameter such as peak particle velocity (Jommi and Pandolfi, 2008; Fleetwood et al., 2009), borehole pressure (Parra, 2012; Duan and Kwok, 2016) or explosion pressure (Ma et al., 2011) is first presented as a critical factor to estimate the size of damage zone, then two different approaches are employed to provide a solution. Either an analytical calculation is used to determine the critical parameter and the damage zone or the relationship between the parameter and the damage zone is estimated and the rest of problem remains unresolved for the reader (Shadabfar et al., 2020). Numerical methods employs algorithm such as finite element method (FEM), finite difference method (FDM), discrete element method (DEM), etc. to evaluate changes in the stress field surrounding an explosion point and examine the resulting induced cracks and damage (Parra et al., 2015; Mitelman and Elmo, 2014; Bendezu et al., 2017). Experimental methods employ laboratory or in-situ tests to develop an empirical relationship to estimate the size and dimension of damages (Onederra et al., 2013).

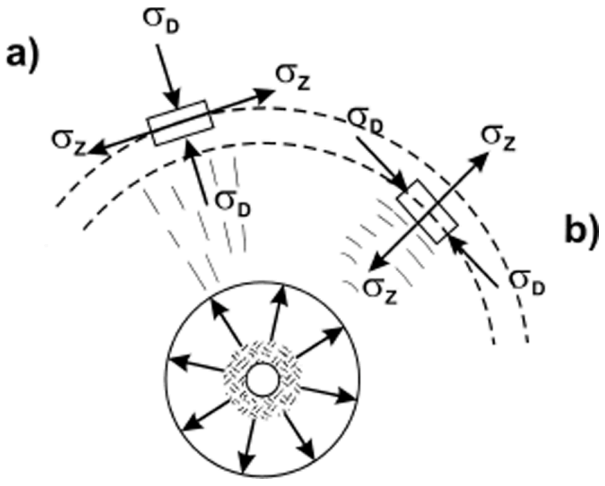

Fig. 9. (a) Radial microfractures created by tangential tensile stress at the front of the P-wave and (b) concentric microfractures generated by the tensile tail at the back of the P-wave (Nielsen and Malvik, 1999).

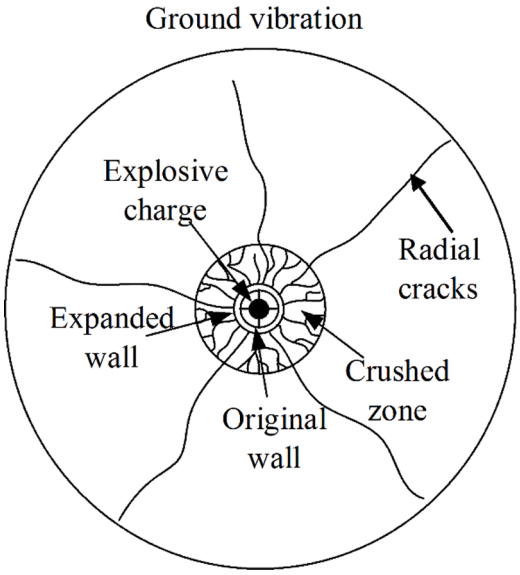

Fig. 10. Damage zones around the blasthole (Shadabfar et al., 2020).

Table 2
Main parameters influencing blast-induced rock damage (Shadabfar et al., 2020).

Type of parameter	Parameter	Description
Rock characteristics	E_d	Young's modulus of rock
	v_d	Poisson's ratio of rock
	σ_c	Uniaxial compressive strength of rock
	F_c	Confined compressive strength of the rock
	T	Tensile strength of the rock
Explosive characteristics	ρ_0	Unexploded explosive density
	D_{CJ}	Ideal detonation velocity
	r_0	Blast hole radius
	Q_{ef}	Effective energy of explosive

An example of an analytical method is Mosinets' model which employs borehole pressure (Shadabfar et al., 2020; Saharan et al., 2006). Mosinets and Gorbacheva (1972) proposed the following equations for estimation of crushed zone, fracture zone and seismic zone based on large diameter borehole studies:

$$\text{Crushed zone radius, } r_c = \sqrt{V_s/V_p} \times \sqrt[3]{q}, \text{mm} \quad (24)$$

$$\text{Fracture zone radius, } r_f = \sqrt{V_p/V_s} \times \sqrt[3]{q}, \text{mm} \quad (25)$$

$$\text{Seismic zone radius, } r_s = \sqrt{V_p/10} \times \sqrt[3]{q}, \text{mm} \quad (26)$$

where V_s is the transverse wave velocity, m/s; V_p is the longitudinal wave velocity, m/s; and q is the explosive weight in TNT equivalent, kg.

4.2.5. Measuring microfractures in the rock fragments

Kranz (1983) and Wong (1985) summarizes the various approaches of characterizing microfractures in rocks to obtain statistical data. The approaches include measuring cracks orientation angles in reference to the applied loading; determining the crack length (l), width (w) and aspect ratios (w/l); measuring crack/fracture densities and counting the number of intersections which a test array of parallel lines make with microcracks in a plane section observed under a microscope. Determination of fracture density is the most common approach. The fracture density may be expressed as the number of cracks per unit volume, the total surface area of cracks per unit volume of the fragmented sample (Nielsen and Malvik, 1999), or the microcrack length per unit area of the sample whereby an appropriate scale is employed such as cm/cm^2 (Nasseri and Mohanty, 2008; Hikita, 2008).

The fracture density in rock fragments may be measured by employing either direct or indirect techniques. The direct techniques employ-two dimensional (2D) and three dimensional (3D) imaging tools to estimate the fracture density (Ghorbani et al., 2011; Liu et al., 2006). The indirect methods are based on the variation of mechanical and elastic properties of the rock fragments and include the study of production in comminution circuits, energy consumption in comminution, Bond's work index test, drop weight test, measurement of P-wave and S-wave velocities, among others. (Galvez, 2011; Parra et al., 2015; Ouchterlony, 2003). Direct methods provide accurate measurement of the microfractures but are limited by the size of samples, are costly, time-consuming and require specialised equipment and skilled personnel (Galvez, 2011; Hikita, 2008). Direct methods are therefore more suitable for small scale analysis of microfractures in the lab. On the other hand, indirect methods are less accurate and involve large sample sizes and are therefore suitable for large scale analysis in the field where huge volumes of fragments are to be analysed (Galvez, 2011).

The traditional 2D imaging tools include light microscope, optical microscope, stereoscopic microscope, scanning electron microscope and fluorescent microscopy in combination with digital image analysis techniques (Hallbauer et al., 1973; Friedman et al., 1970; Seo et al., 2002; Kranz, 1983; Homand et al., 2000; Akesson et al., 2004). The limitations of 2D imaging techniques include stereological error due to poor presentation of the 3D nature of the rock interior, require preparation of the rock sample to obtain a polished surface for the analysis and are consequently destructive (Ghorbani et al., 2011; Guntoro et al., 2020; Liu et al., 2006).

To overcome the limitation of 2D techniques, several approaches have recently been developed for imaging 3D structure of the rock including confocal laser scanning microscopy (CLSM) originally developed for biological community (Liu et al., 2006; Pawley, 2006; Fredrich, 1999), X-ray microtomography (μ-XRT) originally developed for medical use (Ghorbani et al., 2011; Guntoro et al., 2020; Fredrich, 1999; Miller and Lin, 2003), nuclear magnetic resonance imaging (NMRI) also developed for medical use (Doughty and Tomutsa, 1997; Sun et al., 2019; Wang et al., 2020) and 3D synchrotron computed microtomography (Spanne et al., 1994; Wang et al., 2005). Most of the 3D rock structure imaging techniques are more commonly used in other mining-related disciplines such as geology and petroleum engineering to characterize internal structure of drill cores and porous rock (Ghorbani et al., 2011). The μ-XRT is the most widely used 3D imaging technique to quantify microfracture density in rocks (Ghorbani et al., 2011; Parra et al., 2015; Galvez, 2011).

The μ-XRT is a non-destructive and non-invasive 3D imaging technique that employs penetrating X-ray radiations to image the internal features of an opaque object. The technique has been effectively used for several years to visualize characteristics of the interior of solid objects by mapping the attenuation of X-rays through the object (Ghorbani et al., 2011; Willson et al., 2012). The basic principle of its operation is that during scanning of the sample, the X-ray beam passes through the sample as it is rotated around a vertical axis, a proportion of X-rays interacts with the sample thereby decreasing the intensity of (attenuating) the X-rays. The result of the scan is the vertical shadow projections which are graphic files giving information about the amount of X-ray absorption by the sample at a given point (Popov et al., 2020). The difference in X-ray absorption is usually represented in the varying grayscale levels in the detector whereby the more attenuating material in the sample have brighter greyscales. The X-ray attenuation is dependent on the density and composition of the sample and the X-ray energy itself (Guntoro et al., 2020). The shadow vertical projections are then processed by the mathematical transformations into a series of horizontal sections of the sample using a special software and reconstruction of a 3D image of the sample by stacking the transformed horizontal sections (Fig. 11).

For a monochromatic X-ray source, the relationship between the intensity of the incident and attenuated X-rays and the thickness of the sample may be expressed by Beer's law As shown in Eq. (27) (Van Geet et al., 2000; Willson et al., 2012):

$$I = I_0 exp\left[-\left(\frac{\mu}{\rho}\right)\rho t\right] \quad (27)$$

where I is the intensity of attenuated X-ray, I_0 is the intensity of incident X-ray, μ/ρ is the mass linear attenuation coefficient, ρ is the density or concentration of the element in the sample, and t is the voxel thickness.

The linear attenuation coefficient, μ, is a function of the density and the atomic number of the element in the sample and the X-ray energy (Willson et al., 2012) as expressed in Eq. (28) (Van Geet et al., 2001; Van Geet et al., 2000).

$$\mu = \rho\left(a + b\frac{Z^{3.8}}{E^{3.2}}\right) \quad (28)$$

where ρ is the bulk density of the sample, Z is the bulk atomic number of the sample, E is the X-ray energy and a and b are the energy-dependent coefficients.

The first and second term in Eq. (28) corresponds to the physical processes termed as Compton scatter and photoelectric absorption respectively (Van Geet et al., 2000; Curry et al., 1990).

If the sample material or phase is a chemical compound or mixture, its attenuation coefficient is approximated from the coefficients of the constituent elements according to their weighted averages (Willson et al., 2012). For mixtures of atoms in a compound or a mixture, the effective atomic number Z_e is used (Ghorbani et al., 2011; Van Geet et al., 2000) and is expressed as:

$$Z_e = \left(\sum f_i Z_i^{3.8}\right)^{1/3.8} \quad (29)$$

where f_i is the fraction of the total number of electrons contributed by element i and Z_i is the atomic number of element i.

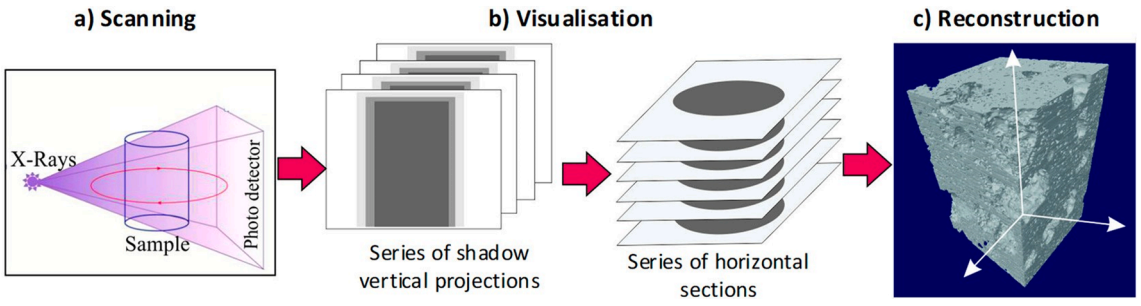

Fig. 11. Basic principles of μ-XRT: (a) scanning of the sample in X-ray beam, (b) mathematical transformation of the shadow vertical projections into a series of horizontal sections of the sample and, (c) creation of 3D image of the sample (Popov et al., 2020).

5. Influence of blasting on productivity of comminution circuits

Numerous studies have demonstrated that the mill throughput can be increased by up to 40 % (Brent et al., 2013) by optimizing blasting operation. The productivity of comminution circuits may be increased either by using a higher specific charge of the explosives or using an explosive with a higher velocity of detonation (Khademian and Bagherpour, 2017; Zhang and Luukkanen, 2021). The use of higher energy explosive results in finer fragmentation and reduction in residual rock strength of fragments due to the higher internal microfracturing, subsequently leading to higher productivity or lower energy consumption of comminution equipment (Michaux and Djordjevic, 2005). For finer and lower strength run-of-mine ore feed material, if the power draw at each stage of comminution is maintained at the same level as with coarser fragmentation feed, then the throughput of the comminution equipment would increase (Nielsen and Malvik, 1999). For comminution circuit employing primary crusher and semi-autogenous (SAG) mill, Michaux and Djordjevic (2005) noted that finer fragmentation of the run-of-mine ore would require smaller crusher gap setting resulting in finer crusher product and subsequently a higher SAG mill throughput. Table 3 shows a summary of some studies conducted by various researchers to investigate the effect of optimizing blasting operations on the mill productivity.

6. Influence of blasting on energy consumption in comminution circuits

6.1. Bond's energy equation

The energy consumption in comminution circuits may be determined by various energy-based comminution models including Rittinger's equation, Kick's equation and Bond's equation. These models express the relationship between energy input to the comminution equipment and the resulting particle size of the product (Wills and Finch, 2015). The Bond's equation is the most commonly used in conventional comminution equipment (Wills and Finch, 2015). The Bond's equation in Eq. (30) may be used to illustrate the relationship between blasting effect and energy consumption in comminution circuits. This equation is employed in comminution to determine the energy required to reduce the ore particle from a given feed size to the desired product size (Workman and Eloranta, 2003).

$$W = 10 \times W_i \left(\frac{1}{\sqrt{P_{80}}} - \frac{1}{\sqrt{F_{80}}} \right) \tag{30}$$

where W is the energy input in kilowatt-hours per metric ton, W_i is the work index in kilowatt-hours per metric ton, and P_{80} and F_{80} are the *80 %* passing size of the product and the feed respectively, in micrometres.

Table 3
Effect of optimizing blasting on mill productivity.

Mine	Blasting Changes	Effect on Mill Productivity	Type of Test	References
Porgera Gold Mine, Papua New Guinea	Blasting powder factor increased from 0.24 to 0.38 kg/tonne by tightening the drill pattern	SAG mill throughput increased from 673 to 774 tonnes/hour (15 % increase)	Modelling, simulation, full-scale validation test	Lam et al. (2001)
Kalgoorlie Consolidated Gold Mine (KCGM), Fimiston Plant, Australia	Powder factor increased from 0.58 to 0.66 kg/tonne, use of a higher VOD and denser explosive	SAG mill throughput increased from 1250 to 1420 tonnes/hour (13.6 % increase)	Modelling, simulation, field investigation	Karageorgos et al. (2001)
Red Dog Mine, Alaska, USA	Powder factor increased from 0.29 to 0.40 kg/tonne Powder factor increased from 0.29 to 0.45 kg/tonne; change of explosive from ANFO to 70/30 emulsion	SAG mill throughput increased from 125 to 132 tonnes/hour (5.6 % increase)SAG mill throughput increased from 125 to 140 tonnes/hour (12 % increase)	Modelling, simulation, field investigation Modelling, simulation, field investigation	Mckee (2013), Paley and Kojovic (2001)
Cadia Hill Mine, Australia	Tightening drill pattern	SAG mill feed rate increased by 12 %	Modelling, simulation	Kanchibotla et al. (1999)
Sandsloot Open Pit Mine, South Africa	Selecting appropriate blasting powder factor for each mining block	Average plant milling rate of autogenous (AG) mill and ball mill improved by 18 %	Modelling, field investigation	Bye (2006)
Boliden Aitik Copper Mine, Sweden	Specific charge increased from 0.92 to 1.36 kg/m^3	AG mill throughput increased by 8 %	Modelling, field investigation	Ouchterlony et al. (2013)
Ban Houayxai Gold-Silver Mine, Laos	Modified bench geometry, blasting patterns and quality control during implementation	Mill throughput for the hard, fresh ore increased by 46 %	Modelling, field investigation	Gaunt et al. (2015)
Gol-e-Gohar Iron Ore Mine, Iran	Powder factor increased from 1650 g/m^3 to 2480 g/m^3 by tightening blasting pattern	SAG mill throughput increases by 30 %. AG mill throughput increases by 5–14 %	Field investigation	Hakami et al. (2015)
Lundin Mining's Chapada Operation, Brazil	Optimization of drill and blast designs for various ore domains as defined by site lithology, rock strength and rock structure	Finer feed to comminution circuit resulted in increase in plant throughput of 13–22 % for soft-fine to hard-coarse ore domains	Modelling, simulation	Glauber et al. (2021)
Gold Fields Cerro Corona copper–gold deposit, Peru	Increasing powder factor by changing the blast design	Average of 14.8 % increase in mill throughput for specific ore types	Modelling, simulation, validation test	La Rosa et al. (2015)

The Bond's equation comprises two parameters for determining the energy required to reduce the sizes of the fragments, namely: (i) the work index that expresses the resistance of the material to comminution and (ii) the particle size reduction required determined by the liberation characteristics of the mineral/metal and the separation techniques to be applied in the subsequent processes (Murr et al., 2015). From the blasting point of view, these two parameters represent the degree of fragmentation of the run-of-mine ore, which serves as the feed to the comminution equipment, attained by blasting. Blasting with higher energy explosive results in finer fragmentation and a higher degree of internal microfracturing in the fragments due to the reduction in strength (work index) of the material (Fig. 12). Considering Bond's equation, Workman and Eloranta (2003) noted that the energy consumption in comminution circuits may be reduced in blasting operation in two ways: reducing the feed size to the primary crusher and decreasing the work index of the material through internal microfracturing.

According to Bond's equation, the work index and particle size distribution of the fragments influence energy consumption in comminution circuits with different magnitude. The particle size in the equation is expressed in the inverse square root meaning that the influence of work index on energy consumption is squared the influence of the particle size of the material (Seccatore, 2019). The equation expresses the relationship between energy consumption and the creation of a new surface area of the particles. Therefore, the higher influence of the work index on energy consumption compared to the particle size of the fragments is due to the higher surface area of internal microfractures in the feed material compared to the surface area of the particles. Revnivtsev (1988) reported that the total surface area of the blast-induced microfractures in rock fragments may range up to 10–100 times greater than the total surface area of the particles.

6.2. Optimization of blasting to reduce energy consumption in comminution

Energy consumption in comminution machines is large compared to drilling and blasting. A study by Doe (2007) reported that comminution expends 44 % (4 % crushing and 40 % grinding) of all the energy consumed in mining operations compared to 7 % for drilling and blasting (5 % drilling and 2 % crushing). Zhang and Luukkanen (2021) and the references therein reported that drilling and blasting together consumes 2 % and crushing and milling expend 53 % of the total energy

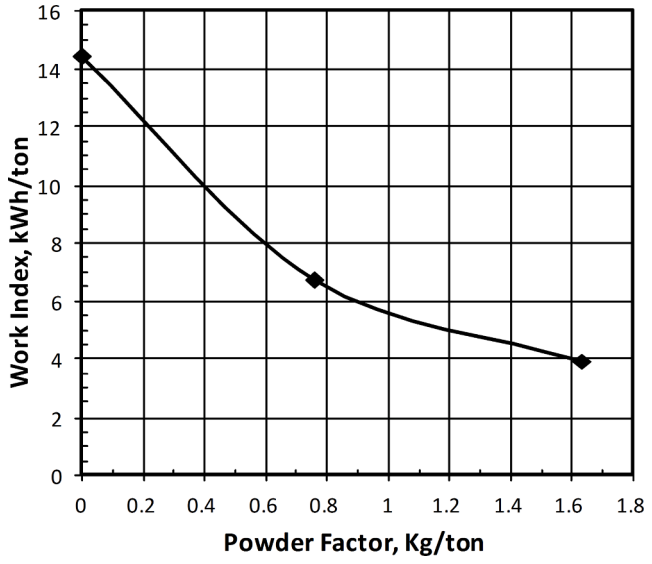

Fig. 12. Relationship between explosive powder factor and work index (Workman and Eloranta, 2003).

input in all mining and processing operations. Workman and Eloranta (2003) conducted a study on blasting and comminution of taconite iron ore and determined the relative energy cost of explosives, crushing and grinding as 5.8 % for explosives, 1.1 % for primary crushing, 2.8 % for secondary crushing and 90 % for grinding. They determined the reduction ratios of primary crushing, secondary crushing and grinding as 4, 5, and 360 respectively. Although these studies give differing figures of energy input in blasting and milling operations, they all generally show that the magnitude of energy expenditure in comminution increases downstream from blasting to grinding operations. The higher energy expenditure in milling compared to blasting may be attributed to the higher reduction ratio achieved and the poor efficiency of grinding equipment in converting electrical energy to actual size reduction. The energy efficiency in grinding machines is estimated as 1 % with the remaining 99 % of the energy expended in moving machinery, generation of heat and noise (Murr et al., 2015; Zhang and Luukkanen, 2021). A study by Eloranta (1997) that compared the efficiency of grinding and blasting estimated 1–2 % efficiency for grinding and 15–30 % efficiency in blasting. Other studies cited by Zhang (2008) estimated that 5–15 % of the energy in blasting is used in rock fragmentation while in grinding the energy utilisation is 1–3 %.

From an environmental and economic point of view, a policy of applying more energy in blasting operations where it is more efficiently utilized and less costly, and conserving it in milling operations where it is less efficient and more costly is essential (Khademian et al., 2017). This can result in significant energy savings in the overall size reduction operations in a mine (Murr et al., 2015; Zhang, 2008; Workman and Eloranta, 2003). Zhang (2008) mathematically demonstrated that the application of more energy in blasting operations results in energy reduction in comminution and overall energy savings in mine operations.

According to Zhang (2008), the energy input and energy utilization in drilling and blasting in conventional mine production are expressed as E_{db} and $\dot{E}_{db}$ respectively. Similarly, the energy input and energy utilization in crushing and grinding are expressed as E_{cg} and $\dot{E}_{cg}$ respectively. Thus, the total energy consumption (E_{tc}) in the whole size reduction from drilling to grinding in conventional mine production is:

$$E_{tc} = E_{db} + E_{cg} \tag{31}$$

The total energy utilized (E_{tu}) to break the rock from drilling to grinding in conventional mine production is:

$$E_{tu} = E_{db}\dot{E}_{db} + E_{cg}\dot{E}_{cg} \tag{32}$$

If the energy input is increased in drilling and blasting by amount Δ and assuming that the energy input in crushing and grinding is reduced by the same amount, then the total energy consumption in the whole size-reduction operation would remain constant.

$$E_{tc} = (E_{db} + \Delta) + (E_{cg} - \Delta) = E_{db} + E_{cg} \tag{33}$$

The total energy utilized to break the rock in the whole size-reduction operation from drilling to grinding after energy distribution changes to:

$$(E_{db} + \Delta)\dot{E}_{db} + (E_{cg} - \Delta)\dot{E}_{cg} = E_{tu} + (\dot{E}_{db} - \dot{E}_{cg})\Delta \tag{34}$$

By substituting Eq. (32) into Eq. (34) we get:

$$E^{*}_{tu} = E_{tu} + (\dot{E}_{db} - \dot{E}_{cg})\Delta \tag{35}$$

Eq. (35) shows that there is an additional energy of upto $(\dot{E}_{db} - \dot{E}_{cg})\Delta$ utilized in the whole size-reduction system after energy redistribution even though the total energy input is not changed. If energy Δ is moved from crushing and grinding to drilling and blasting, energy wastage is reduced by upto $(\dot{E}_{db} - \dot{E}_{cg})\Delta$ in the whole size-reduction system (Zhang and Luukkanen, 2021). Energy input in drilling and blasting may be increased in several ways; the most popular ways

include increasing powder factor, changing blasting agents to ones with higher VOD and improving the distribution of blasting energy (Murr et al., 2015). Table 4 shows a summary of some studies conducted to investigate the effect of optimizing blasting on energy consumption in comminution equipment.

7. Influence of blasting on metal leaching

7.1. Factors influencing leaching performance

Leaching in mineral extraction refers to selective dissolution of a metal/mineral of interest in an aqueous solution using a suitable lixiviant (Marsden and House, 2006). Various techniques of leaching exist including heap leaching, dump leaching, in-situ leaching, agitation leaching, pressure leaching, and vat leaching (Schlesinger et al., 2011; Gupta, 2006; Marsden and House, 2006). The choice of a particular technique mainly depends on the mineralogy of the ore, the relationship between particle size of the fragments and mineral recovery, grade of the ore, environmental considerations, availability of capital financing, among other factors (Scheffel, 2002; Marsden and House, 2006).

Leaching performance may be evaluated by three indicators including leaching kinetics, reagent consumption and metal recovery (Free, 2013; Marsden and House, 2006; Parra et al., 2015). The rate of metal dissolution is influenced by factors such as the exposed surface area of the target metal values, concentration of the leaching reagents, pH, temperature, grade of the metal value in the ore, degree of agitation and mass transport, nature of the gangue mineral and presence of other ions in the solution (Marsden and House, 2006; Parra et al., 2015). Reagents consumption is mainly influenced by chemical aspects of the target metal values and the gangue minerals and type of the solvent used (Parra et al., 2015). Factors influencing mineral recovery include exposed surface area of the target metal value, concentration of the reagents, residence time, pH of the solution, and association of the metal values with the gangue minerals.

A common factor influencing leaching performance in the three indicators is the exposed surface area of the metal values and the gangue minerals. The exposed surface area of the metal values is dependent on the particle size distribution of the fragments, liberation characteristics of the ore influenced by the efficiency of comminution operations preceding leaching, and the permeability of fragments influenced by the internal microfractures and the natural porosity of the ore (Marsden and House, 2006; Parra et al., 2015).

The rate of metal dissolution and metal recovery generally increases with decreasing fragment particle sizes due to the increase in liberation and surface area of mineral values and the increase in permeability of the ore fragments caused by internal microfracturing (Marsden and House, 2006). However, decreasing particle size of the ore and increasing its permeability by higher energy blasting may also lead to higher reagent consumption, lower dissolution rate and eventually lower recovery due to the increased exposure of problematic gangue minerals such as cyanicides in gold ores (Marsden and House, 2006). Therefore, fragment conditioning by blasting should only improve the exposure of the target mineral values without increasing the gangue exposure (Parra et al., 2015). For coarse fragments treated in heap and dump leaching operations, the main factor that influences mineral exposure is the internal fractures that can be induced by blasting (Parra et al., 2015).

7.2. Influence of blast-induced microfracturing on metal recovery

Numerous studies have been conducted over the years to determine the influence of particle size of fragments on leaching recovery (Lwambiyi et al., 2009; Wen et al., 1996; Ofosuhene and Abaka-Wood, 2020; Egan et al., 2016; Ruan et al., 2019; Zhou et al., 2019). However, fewer research studies have been conducted on the influence of internal fractures. The type of fractures induced by blasting may influence mineral liberation and recovery (Hikita, 2008). If blasting preferentially generates intergranular fractures, mineral liberation would be enhanced, leading to improved recovery in separation processes such as flotation (Hikita, 2008; Ouchterlony, 2003). Conversely, intragranular fractures may hinder mineral liberation and reduce flotation recovery (Hikita, 2008). A high number of intragranular fractures will increase permeability and exposure of mineral values to leaching reagents leading to high metal recovery (Galvez, 2011; Parra et al., 2015).

Fribla (2006) investigated the effect of increasing blasting energy on generation of micro-cracks in the oxidised copper ores and the subsequent effect on copper leaching recovery. A one-stage crushing of the samples blasted with different powder factors was employed. The samples blasted with higher powder factors yielded higher copper recoveries due to the higher degree fragment conditioning. However, Parra et al. (2015) comments that the study did not differentiate the effect of increased microfracturing from the increased proportion of fines on the copper recovery when blasting the samples with higher powder factor.

Parra et al. (2015) studied the effect of fragment conditioning by blasting a leachable synthetic material on copper recovery. After blasting, the fragment samples were collected from different zones around the explosive charge which corresponded to different degrees of conditioning. The samples were subjected to X-ray tomography tests to determine the degree of microfracturing and cyanide leaching tests to determine recovery. The fractures generated in the samples were transgranular (62 %), intergranular (35 %) and intragranular (3 %). Copper recovery in low conditioning zones of blasted samples was

Table 4
Effect of optimizing blasting on energy consumption in comminution equipment.

Material	Blasting changes	Effect on energy consumption	Type of test	References
Gold ore	Powder factor increased from 0.72 to 1.46 kg/m^3	Overall energy consumption in comminution circuits decreased from 23.8 to 17.3 kWh/t	Full-scale field test	Kanchibotla et al. (2015)
Metal ore	Powder factor increased by 25 %	Energy cost in mining and comminution reduced by 10 %	Full-scale field test	Fuerstenau et al. (1995)
Gold ore	Powder factor increased by 33 %	SAG mill energy consumption reduced by 29 %	Full-scale field test	Kanchibotla and Valery (2010)
Gold ore	Powder factor increased by 40 %	Grinding cost reduced by 19 %	Full-scale field test	Kruttschnitt (2000)
Copper ore	Powder factor increased by 20 % by tightening blasting pattern; explosives cost increased by 0.04 US Dollars per ton	Mill energy consumption decreased by 25 % resulting in 0.1 US Dollars per ton mill energy cost saving	Full-scale field test	Asgari and Farshad (2015)
Copper-gold deposit	Powder factor increased by changing blast design	Grinding energy consumption reduced by 12 %	Modelling, simulation, field validation test	La Rosa et al. (2015)
Iron ore deposit	Powder factor increased by 50 % by tightening blasting pattern	Mill energy consumption decreased by 4 to 21 %	Field investigation	Hakami et al. (2015)
Granite blocks	Substituting ANFO with pentolite and emulite explosives of higher VOD	Bond work index reduced by 9.2 % for pentolite and 6.7 % for emulate	Laboratory study	Khademian and Bagherpour (2017)

almost the same as in the unblasted material. In the intermediate conditioning zones, the copper recovery increased by 0.84 % compared to low conditioning zones. The low recovery in the intermediate and low conditioning zones was due to the small proportion of intragranular fractures that cut the grain matrix to expose a significant amount of metal values to leaching reagents.

The exposure of mineral values to the leaching reagents is not only influenced by the presence of microfractures but also by the grain size of the mineral values (which can be significantly smaller than the gangue minerals), grain shapes of the minerals and the nature of association of the mineral values with the gangue minerals (Parra et al., 2015). The mineral grain sizes, grain shape and mineral associations at microscale are termed as 'mineral textures' (Lund et al., 2014). Mineral textures influence the metallurgical behaviour of the ore including comminution, liberation and recovery (Bonnici et al., 2008). Blast-induced fragment conditioning increases the probability of improving the recovery depending on the extent to which the microfractures expose the mineral values (Parra et al., 2015). The degree of this exposure is dependent on the type of microfractures induced by blasting and the textural characteristics of the ore. Therefore, further research should focus on establishing the relationship between blast intensity and metal leaching recovery for metal ores of different textural attributes. The findings of such research would help in optimizing blasting operations to improve metal recoveries in heap and dump leaching.

8. Conclusions

The degree of rock fragmentation in bench blasting operations in metal mines is influenced by the controllable factors including the blast geometry and the explosive properties and the uncontrollable factors which include the rockmass properties and the environmental and safety constraints. In processing of metal ores, the two important aspects of blast fragmentation include the particle size distribution of the muckpile fragments and the internal microfractures induced by blasting. Consequently, the degree of rock fragmentation in metal mines may be evaluated in terms of the particle size distribution of the fragments and the degree of blast-induced microfracturing in the fragments.

Fragment size distribution may be assessed either by the cumulative size distribution curves of the experimentally-determined particle size analysis data or by the fragment size distribution models. The degree of microfracturing induced in the rock fragments may be quantified in terms of the fracture density which can be measured either directly or indirectly. The direct methods employs 2D or 3D imaging techniques to estimate the fracture density. The 3D imaging techniques offer more advantages over the 2D techniques including better presentation of the 3D nature of the rock, are non-destructive and require minimal preparation of the rock samples for the analysis. The X-ray microtomography is the most popular 3D imaging technique used to estimate the microfracture density in rocks.

Increase in blasting energy results in finer fragmentation and higher degree of microfracturing in the rock fragments. This consequently increases the productivity of comminution equipment, reduces the energy consumption in comminution equipment and may increase the metal recovery. However, the blasting energy should only be increased upto a level that yields the minimum negative environmental and safety impacts.

Energy consumption in comminution machines is large compared to energy used in drilling and blasting. Energy utilization in comminution is lower than energy utilization in blasting. Therefore, redistribution of energy in comminution to blasting results in overall energy savings in mining operations.

Finer fragmentation increases the liberation of metal values from the gangue. Higher internal microfracturing increases permeability of the ore fragments hence increasing the exposure of the contained metal values to leaching reagents, leading to the improvement in metal recovery. The influence of blasting on leaching recovery is particularly more pronounced in heap and dump leaching operations which employ only one stage of comminution. The type of microfractures induced in rock fragments by blasting influence the metal leaching recovery. A higher proportion of intragranualar fractures may increase the permeability of the ore fragments and consequently increase the metal recovery.

The exposures and the recoveries of metal values are not only influenced by the predominant type of microfractures induced but also by the nature of mineral textures including the mineral grain sizes and shapes and the forms of association of the metal values with the gangue minerals. Thus, blast-induced conditioning only increases the probability of improving the metal recovery by favourably exposing the metal values to the leaching reagents. Further research should be conducted to establish the relationship between blasting energy and metal leaching recovery in the ores of different textural attributes.

CRediT authorship contribution statement

Eric Munene Kinyua: Conceptualization, Methodology, Writing – original draft, Writing – review & editing. **Zhang Jianhua:** Supervision. **Richard M. Kasomo:** Writing – review & editing, Resources. **Dalmus Mauti:** Writing – review & editing. **Jackson Mwangangi:** Conceptualization, Writing – review & editing.

Declaration of Competing Interest

The authors declare that they have no known competing financial interests or personal relationships that could have appeared to influence the work reported in this paper.

Data availability

No data was used for the research described in the article.

References

Adebayo, B., Akande, J., 2015. Effects of blast-hole deviation on drilling and muck-pile loading cost. Int. J. Sci. Res. Innov. Technol. 2, 64–73.

Adhikari, G., Theresraj, A., Venkatesh, H., Balachander, R., Gupta, R., 2004. Ground vibration due to blasting in limestone quarries. Fragblast 8, 85–94.

Agyei, G., Nkrumah, M., 2021. A review on the prediction and assessment of powder factor in blast fragmentation. Nigerian J. Technol. 40, 275–283.

Agyei, G., Owusu-Tweneboah, M., 2019. A Comparative Analysis of Rock Fragmentation using Blast Prediction Results. Ghana Min. J. 19, 49–58.

Akesson, U., Hansson, J., Stigh, J., 2004. Characterisation of microcracks in the Bohus granite, Western Sweden, caused by uniaxial cyclic loading. Eng. Geol. 72, 131–142.

Anders, M.H., Laubach, S.E., Scholz, C.H., 2014. Microfractures: A review. J. Struct. Geol. 69, 377–394.

Asgari, A.R., Farshad, Norouzi, Sanaz., 2015. Blast-Induced Rock Fracturing and Minimizing Downstream Comminution Energy Consumption.

Ash, R.L., 1968. The design of blasting rounds. Surface Min. 387.

Asl, P.F., Monjezi, M., Hamidi, J.K., Armaghani, D.J., 2018. Optimization of flyrock and rock fragmentation in the Tajareh limestone mine using metaheuristics method of firefly algorithm. Eng. Comput. 34, 241–251.

Ayaga, K.B., 2016. Comparative Analysis of Rock Fragmentation Models: A Case Study. Master of Philosophy in Mining Engineering. University of Mines and Technology (UMaT), Tarkwa.

Aziznejad, S., Esmaeili, K., 2015. Effects of joint intensity on rock fragmentation by impact. In: Proceedings of 11th international symposium on rock fragmentation by blasting, Sydney, NSW, 24-26.

Banadaki, M.D., Mohanty, B., 2012. Numerical simulation of stress wave induced fractures in rock. Int. J. Impact Eng. 40, 16–25.

Bendezu, M., Romanel, C., Roehl, D., 2017. Finite element analysis of blast-induced fracture propagation in hard rocks. Comput. Struct. 182, 1–13.

Bergmann, O., Riggle, J., Wu, F., 1973. Model rock blasting—effect of explosives properties and other variables on blasting results. Int. J. Rock Mech. Min. Sci. Geomech.. Elsevier, 585-612.

Bhandari, S., 1997. Engineering rock blasting operations. Balkema, Rotterdam, Netherlands, A. A.

Blair, D., 2004. Curve-fitting schemes for fragmentation data. Fragblast 8, 137–150.

Bonnici, N., Hunt, J.A., Walters, S., Berry, R.F., Collett, D., 2008. Relating textural attributes to mineral processing: Developing a more effective approach for the Cadia East Cu-Au porphyry deposit.

Brady, B.H., Brown, E.T., 2006. Rock mechanics for underground mining. Springer Science & Business Media.

Brent, G., Rothery, M., Dare-Bryan, P., Hawke, S., Gomez, R., Humeres, I., 2013. Ultra-high intensity blasting for improved ore comminution. Rock Fragmentation by Blasting: The 10th International Symposium on Rock Fragmentation by Blasting, 2012 (Fragblast 10). Taylor & Francis Books Ltd, 163-169.
Burkle, W., 1980. Geology and its effect on blasting. Pit Quarry;(United States), 73.
Bye, A., 2006. The strategic and tactical value of a 3D geotechnical model for mining optimization, Anglo Platinum, Sandsloot open pit. J. South Afr. Inst. Min. Metall. 106, 97–104.
Chakraborty, A., Jethwa, J., Paithankar, A., 1994. Effects of joint orientation and rock mass quality on tunnel blasting. Eng. Geol. 37, 247–262.
Chi, L.Y., Zhang, Z.X., Aalberg, A., Yang, J., Li, C.C., 2019. Measurement of shock pressure and shock-wave attenuation near a blast hole in rock. Int. J. Impact Eng. 125, 27–38.
Chiappetta, R.F., 1998a. Choosing the right delay timing for the blasting application, optimization and maintaining field control. Proceedings of 8th High-Tech Seminar on State-of-the Art, Blasting Technology, Instrumentation and Explosives Applications, 215-254.
Chiappetta, R.F., 1998b. Blast monitoring instrumentation and analysis techniques, with an emphasis on field applications. Fragblast 2, 79–122.
Cho, S.H., Nishi, M., Yamamoto, M., Kaneko, K., 2003. Fragment size distribution in blasting. Mater. Trans. 44, 951–956.
Choudhary, B.S., 2013. Firing patterns and its effect on muckpile shape parameters and fragmentation in quarry blasts. Int. J. Res. Eng. Technol. 2, 32–45.
Chung, S.H., Katsabanis, P., 2000. Fragmentation prediction using improved engineering formulae. Fragblast 4, 198–207.
Coello-Velázquez, A.L., Quijano, A.V., Menéndez-Aguado, J.M., Pole, F.M., Llorente, L., 2019. Use of the Swebrec Function to Model Particle Size Distribution in an Industrial-Scale Ni-Co Ore Grinding Circuit. Metals 9, 882.
Cunningham, C., 1983. The Kuz-Ram Model for production of fragmentation from blasting. In: Proc. Symp. on Rock Fragmentation by Blasting, Lulea.
Cunningham, C., 1987. Fragmentation estimations and the Kuz-Ram model-four years on. In: Proc. 2nd int. symp. on rock fragmentation by blasting, 475–487.
Cunningham, C., 2005. The Kuz-Ram fragmentation model–20 years on. Brighton conference proceedings. European Federation of Explosives Engineers, England, 201–210.
Curry, T.S., Dowdey, J.E., Murry, R.C., 1990. Christensen's physics of diagnostic radiology. Lippincott Williams & Wilkins.
Da Gama, D., 1983. Use of comminution theory to predict fragmentation of jointed rock mass subjected to blasting. Proc. First Int. Symp. on Rock Frag. By Blasting, Lulea, Sweden, 563-579.
Dinis Da Gama, C., Jimeno, L.C., 1993. Rock fragmentation control for blasting cost minimization and environmental impact abatement. International symposium on rock fragmentation by blasting, 273-280.
Djordjevic, N.A., 1999. Two-component model of blast fragmentation. AusIMM Proceedings, 9-13.
Doe, U., 2007. Mining industry energy bandwidth study. Washington DC: Prepared by BCS.
Dotto, M.S., Pourrahimian, Y., 2018. Effects of Fragmentation Size Distribution on Truck-Shovel Productivity. Mining Optimization Laboratory, University of Alberta, Edmonton, Canada.
Doughty, D., Tomutsa, L., 1997. Imaging pore structure and connectivity by high resolution NMR microscopy. Int. J. Rock Mech. Min. Sci. 34, 69. e1-69. e10.
Duan, K., Kwok, C., 2016. Evolution of stress-induced borehole breakout in inherently anisotropic rock: Insights from discrete element modeling. J. Geophys. Res. Solid Earth 121, 2361–2381.
Dunford, J.. n.d. Control and Prediction of Blast Fragmentation and its Impact on Comminution. Camborne School of Mines Association.
Egan, J., Bazin, C., Hodouin, D., 2016. Effect of particle size and grinding time on gold dissolution in cyanide solution. Minerals 6, 68.
Elahi, A.T., Hosseini, M., 2017. Analysis of blasted rocks fragmentation using digital image processing (case study: limestone quarry of Abyek Cement Company). Int. J. Geo-Eng. 8, 1–11.
Eloranta, J., 1997. The efficiency of blasting versus crushing and grinding. Proceedings of the 23rd Conference of Explosives and Blasting Technique, 1-7.
Esen, S., 2013. Fragmentation modelling and the effects of ROM fragmentation on comminution circuits. International Mining Congress & Extibition of Turkey, 251-260.
Fernández, P.R., Rodríguez, R., Bascompta, M., 2022. Holistic Approach to Define the Blast Design in Quarrying. Minerals 12, 191.
Fleetwood, K.G., Villaescusa, E., Li, J., 2009. Limitations of using PPV damage models to predict rock mass damage. Proceedings of the Thirty-Fifth Annual Conference on Explosives and Blasting Technique, Denver, CO, USA, 8-11.
Fredrich, J., 1999. 3D imaging of porous media using laser scanning confocal microscopy with application to microscale transport processes. Phys. Chem. Earth Part A. 24, 551–561.
Free, M., 2013. Hydrometallurgy: fundamentals and applications. John Wiley & Sons.
Fribla, H., 2006. Microfracturing as a result of explosion and increased dissolution of metal in an oxidized copper ore. 8th International Symposium on Rock Fragmentation by Blasting, Editec SA, Santiago, Chile, 262-270.
Friedman, M., Perkins, R., Green, S., 1970. Observation of brittle-deformation features at the maximum stress of Westerly granite and Solenhofen limestone. Int. J. Rock Mech. Min. Sci. Geomech. Elsevier, 297-302.
Fuerstenau, M., Chi, G., Bradt, R., 1995. Optimization of energy utilization and production costs in mining and ore preparation processes. Society for Mining, Metallurgy, and Exploration, Inc., Littleton, CO.
Galvez, H.I.P., 2011. Analysis of the state of the art of blast-induced fragment conditioning. Miner. Eng. 24, 1638–1640.
Gates, A., 1915. Kick vs. Rittinger: an experimental investigation in rock crushing performed at Purdue University. Trans AIME 52, 875–909.
Gaudin, A., 1926. An investigation of crushing phenomena. Trans. Am. Instit. Min. Metall. Eng. 73, 253–316.
Gaunt, J., Symonds, D., Mcnamara, G., Adiyansyah, B., Kennelly, L., Sellers, E., Kanchibotla, S., 2015. Optimisation of drill and blast for mill throughput improvement at ban houayxai mine. 11th international symposium on rock fragmentation by blasting, 307-314.
Gheibie, S., Aghababaei, H., Hoseinie, S., Pourrahimian, Y., 2009. Modified Kuz—Ram fragmentation model and its use at the Sungun Copper Mine. Int. J. Rock Mech. Min. Sci. 46, 967–973.
Ghorbani, Y., Becker, M., Petersen, J., Morar, S.H., Mainza, A., Franzidis, J.P., 2011. Use of X-ray computed tomography to investigate crack distribution and mineral dissemination in sphalerite ore particles. Miner. Eng. 24, 1249–1257.
Gilvarry, J.J., 1961. Fracture of brittle solids. I. Distribution function for fragment size in single fracture (theoretical). J. Appl. Phys. 32, 391–399.
Gilvarry, J., Bergstrom, B., 1961. Fracture of brittle solids. II. Distribution function for fragment size in single fracture (experimental). J. Appl. Phys. 32, 400–410.
Glauber, E.A.M., Moura, F., Souza, I., Resende, F., Henrique, P.J.C., Ribeiro, A., Valery, W., Valle, R., Plasencia, R.H., 2021. Integrated Optimization of Drill & Blast, and Comminution Processes at Lundin Mining -Chapada. The 17th International Conference on Mineral Processing and Geometallurgy, Procemin-Geomet, October 20 -22, 2021 Virtual, online.
Grady, D.E., 1990. Particle size statistics in dynamic fragmentation. J. Appl. Phys. 68, 6099–6105.
Grady, D., Kipp, M., 1985. Geometric statistics and dynamic fragmentation. J. Appl. Phys. 58, 1210–1222.
Griffith, A.A., 1920. The phenomenon of rupture and flow in solids. Phil. Trans. Royal Soc London, A. 221, 163–198.
Grundstrom, C., Kanchibotla, S., Jankovich, A., Thornton, D., Pacific, D.D.N.A., 2001. Blast fragmentation for maximising the sag mill throughput at Porgera Gold Mine. Proceedings of the annual conference on explosives and blasting technique. ISEE; 1999, 383-400.
Guntoro, P.I., Ghorbani, Y., Butcher, A.R., Kuva, J., Rosenkranz, J., 2020. Textural Quantification and Classification of Drill Cores for Geometallurgy: Moving Toward 3D with X-ray Microcomputed Tomography (μCT). Nat. Resour. Res. 29, 3547–3565.
Gupta, C.K., 2006. Chemical metallurgy: principles and practice. John Wiley & Sons.
Hagan, T., 1983. The influence of controllable blast parameters on fragmentation and mining costs. Proceedings of the 1st international symposium on rock fragmentation by blasting, 31-32.
Hagan, T., 1995. The effect of rock properties on the design and results of tunnel blasts. J. Rock Mech. Tunnell. Technol. 1, 25–39.
Hakami, A., Mansouri, H., Farsangi, E., Dehghan, M., Faramarzi, F., 2015. Study of the effect of blast pattern design on autogenous and semi-autogenous mill throughput at gol-e-gohar iron ore mine.
Hallbauer, D., Wagner, H., Cook, N., 1973. Some observations concerning the microscopic and mechanical behaviour of quartzite specimens in stiff, triaxial compression tests. Int. J. Rock Mech. Min. Sci. Geomech. Abstr. Elsevier, 713-726.
Hemphill, G.B., 1981. Blasting operations. McGraw-Hill Companies.
Hikita, D.H., 2008. The influence of blasting on Kemess hypogene ore milling. Masters International.
Holmberg, R., 1974. Charge calculations for bench blasting. SveDeFo report. Swedish Detonic Research Foundation, Stockholm.
Homand, F., Hoxha, D., Belem, T., Pons, M.N., Hoteit, N., 2000. Geometric analysis of damaged microcracking in granites. Mech. Mater. 32, 361–376.
Hu, Y.G., Liu, M.S., Wu, X.X., Zhao, G., Li, P., 2018. Damage-vibration couple control of rock mass blasting for high rock slopes. Int. J. Rock Mech. Min. Sci. 103, 137–144.
Hüdaverdİ, T., Akyildiz, Ö., 2020. Investigation of Blast Fragmentation Models in a Sandstone Quarry. Bilimsel Madencilik Dergisi 59, 145–156.
Janković, A., Valery, W., 2002. Mine to mill optimisation for conventional grinding circuits: A scoping study. J. Min. Metall. A: Min. 38, 49–66.
Jimeno, C.L., Jimeno, E.L., Carcedo, F.J.A., De Ramiro, Y.V., 1995. Drilling and Blasting of Rocks, BR Rotterdam, Netherlands, A. A. Balkema.
Jommi, C., Pandolfi, A., 2008. Vibrations induced by blasting in rock: a numerical approach. Rev Ital Geotec 20, 77–94.
Kabwe, E., 2018. Velocity of detonation measurement and fragmentation analysis to evaluate blasting efficacy. J. Rock Mech. Geotech. Eng. 10, 523–533.
Kanchibotla, S., Morrell, S., Valery, W., O'loughlin, P., 1998. Exploring the effect of blast design on SAG mill throughput at KCGM. Mine to Mill Conference, Australasian Institute of Mining and Metallurgy, Brisbane, Australia, 153-158.
Kanchibotla, S., Valery, W., 2010. Mine-to-mill process integration and optimization–benefits and challenges. Annual Conference on Explosives and Blasting Technique 7–10.
Kanchibotla, S., Valery, W. & Morrell, S., 1999. Modelling fines in blast fragmentation and its impact on crushing and grinding. Explo '99–A conference on rock breaking, The Australasian Institute of Mining and Metallurgy, Kalgoorlie, Australia, 137-144.
Kanchibotla, S., Vizcarra, T., Musunuri, S., Tello, S., Hayes, A., Moylan, T., 2015. Mine to mill optimisation at paddington gold operations. International conference on semi-autogenous and high pressure grinding technology.
Karageorgos, J., Skrypniuk, J., Valery, W., Ovens, G., 2001. SAG milling at the Fimiston plant (KCGM). SAG 2001, 109–124.
Khademian, A., Bagherpour, R., 2017. Alteration of grindability of minerals due to applying different explosives in blasting operation. Miner. Eng. 111, 174–181.

Khademian, A., Bagherpour, R., Almasi, S., Jamali, S., 2017. Preconditioning effect of blasting and its role in mineral extraction chain. 25th International Mining Congress and Exhibition of Turkey, Antalya, Turquía.
Kondelchuk, D., Novikov, E., 2005. Study of the mechanical properties of the granitoid rocks and the influence of blasting parameters on the quality of aggregates: Literature Research.
Konya, A., Konya, C.J., 2019. Blasting mechanics revisited: Blasting design standards. https://www.pitandquarry.com/blasting-mechanics-revisited-blasting-design-standards/ (accessed 6 May 2022).
Koulli, S.P., 1993. Computerized design and result prediction of bench blasting. International symposium on rock fragmentation by blasting, 263-271.
Kranz, R.L., 1983. Microcracks in rocks: a review. Tectonophysics 100, 449–480.
Kruttschnitt, S., 2000. Mine to mill blasting to maximize the profitability of mineral industry operations. In: Proceedings of The Annual Conference on Explosives and Blasting Technique. ISEE; 1999, 349-360.
La Rosa, D., Caron, K., Valery, W., Diaz, R., Mamani, H., 2015. Blast fragmentation impacts on downstream processing at Goldfields Cerro Corona.
Lam, M., Jankovic, A., Valery, W., Kanchibotla, S., 2001. Maximising sag mill throughput at porgera gold mine by optimising blast fragmentation.
Larsson, B., 1974. Report on blasting of high and low benches—fragmentation from production blasts. In: Proceedings of discussion meeting BK74, Swedish Rock Construction Committee, Stockholm, 247-273.
Leng, Z., Fan, Y., Gao, Q., Hu, Y., 2020. Evaluation and optimization of blasting approaches to reducing oversize boulders and toes in open-pit mine. Int. J. Min. Sci. Technol. 30, 373–380.
Liu, S., Anwar, A.F., Kim, B.C., Ichikawa, Y., 2006. Observation of microcracks in granite using a confocal laser scanning microscope. Int. J. Rock Mech. Min. Sci. 43, 1293–1305.
Lógó, B.A., Vásárhelyi, B., 2019. Estimation of the Poisson's rate of the intact rock in the function of the rigidity. Periodica Polytechnica Civ. Eng. 63, 1030–1037.
Lu, P., Latham, J.P., 1998. A model for the transition of block sizes during fragmentation blasting of rock masses. Fragblast 2, 341–368.
Lund, C., Lamberg, P., Lindberg, T., A new method to quantify mineral textures for geometallurgy. Process Mineralogy: 17/11/2014-19/11/2014, 2014.
Lwambiyi, M., Maweja, K., Kongolo, K., Lwambiyi, N.M., Diyambi, M., 2009. Investigation into the heap leaching of copper ore from the Disele deposit. Hydrometallurgy 98, 177–180.
Lyana, K.N., Hareyani, Z., Shah, A.K., Hazizan, M.M., 2016. Effect of geological condition on degree of fragmentation in a Simpang Pulai marble quarry. Procedia Chem. 19, 694–701.
Ma, G., Hao, H., Wang, F., 2011. Simulations of explosion-induced damage to underground rock chambers. J. Rock Mech. Geotech. Eng. 3, 19–29.
Maiti, K., Kayal, S., 2020. Estimating Reliability Characteristics of the Log-Logistic Distribution Under Progressive Censoring with Two Applications. Ann. Data Sci. 1–40.
Marsden, J., House, I., 2006. The chemistry of gold extraction, SME.
Marton, A., Crookes, R.A., 2001. Case study in optimising fragmentation. Proceedings of the Australasian Institute of Mining and Metallurgy 2000. Parkville, 35-44.
Mckee, D., 2013. Understanding mine to mill: The Cooperative Research Centre for Optimising Resource Extraction, Brisbane, AU, 96 p.
Mckenzie, C., 2013. Seed wave modelling applications for fragmentation, damage, and environmental impact control. Blasting mines—new trends Taylor Fr London.
Michaux, S., Djordjevic, N., 2005. Influence of explosive energy on the strength of the rock fragments and SAG mill throughput. Miner. Eng. 18, 439–448.
Miller, J., Lin, C., 2003. 3D Analysis of particulates in mineral processing systems by cone beam x-ray microtomography. XXII International Mineral Processing Congress, Cape Town, South Africa. Citeseer.
Mishra, A., 2009. Designing of Surface Blasts-A Computational Approach.
Mitelman, A., Elmo, D., 2014. Modelling of blast-induced damage in tunnels using a hybrid finite-discrete numerical approach. J. Rock Mech. Geotech. Eng. 6, 565–573.
Mohamed, F., Riadh, B., Abderazzak, S., Radouane, N., Ibsa, T., 2019. Distribution analysis of rock fragments size based on the digital image processing and the Kuz-Ram model Cas of Jebel Medjounes quarry. Aspects Min. Mineral Sci. 2.
Mosinets, V., Gorbacheva, N., 1972. A seismological method of determining the parameters of the zones of deformation of rock by blasting. Soviet Min. Sci. 8, 640–647.
Mulenga, S., 2020. Evaluation of factors influencing rock fragmentation by blasting using interrelations diagram method. J. Phys. Sci. 2, 1–16.
Müller, B., Hausmann, J., Niedzwiedz, H., 2009. Control of rock fragmentation and muck pile geometry during production blasts (environmentally friendly blasting technique). Proceedings of 9th rock fragmentation by blasting symposium, Frgagblast, 277–286.
Murr, D., Workman, L., Eloranta, J., Katsabanis, P., 2015. Blasting influence on comminution. SAG Conference, 1-21.
Nasseri, M., Mohanty, B., 2008. Fracture toughness anisotropy in granitic rocks. Int. J. Rock Mech. Min. Sci. 45, 167–193.
Nielsen, K., Kristiansen, J., 2020. Blasting-crushing-grinding: Optimisation of an integrated comminution system. Rock fragmentation by blasting. CRC Press.
Nielsen, K., Malvik, T., 1999. Grindability enhancement by blast-induced microcracks. Powder Technol. 105, 52–56.
Nirm, 2001. Evaluation of Explosives Performance through In-The-Hole Detonation Velocity Measurement. National Institute of Rock Mechanics (NIRM).
Nobel, D., 2010. Blasting and explosives quick reference guide. Dyno Nobel Asia Pacific Pty Limited, Kalgoorlie.
Obert, L., Duvall, W.I., 1967. Rock mechanics and the design of structures in rock. Wiley, New York.
Ofosuhene, N., Abaka-Wood, G.B., 2020. A study of the effect of changes in leach feed particle size on gold recovery from low-grade ores. 6th UMaT Biennial International Mining and Mineral Conference. Tarkwa, Ghana.
Olofsson, S.O., 1990. Applied explosives technology for construction and mining, Applex.
Olsson, M., Nie, S., Bergqvist, I., Ouchterlony, F., 2002. What causes cracks in rock blasting? Fragblast 6, 221–233.
Onederra, I.A., Furtney, J.K., Sellers, E., Iverson, S., 2013. Modelling blast induced damage from a fully coupled explosive charge. Int. J. Rock Mech. Min. Sci. 58, 73–84.
Ouchterlony, F., 2005a. The Swebrec© function: linking fragmentation by blasting and crushing. Min. Technol. 114, 29–44.
Ouchterlony, F., Bergman, P., Nyberg, U., 2013. Fragmentation in production rounds and mill through-put in the Aitik copper mine, a summary of development projects 2002–2009. Rock Fragmentation by Blasting: The 10th International Symposium on Rock Fragmentation by Blasting, 2012 (Fragblast 10). Taylor & Francis Books Ltd, 117-128.
Ouchterlony, F., Niklasson, B., Abrahamsson, S., 1990. Fragmentation monitoring of production blasts at MRICA. International Symposium on Rock Fragmentation by Blasting: 26/08/1990-31/08/1990. The Australian Institute of Mining and Metallurgy, 283-289.
Ouchterlony, F., Sanchidrián, J.A., 2019. A review of development of better prediction equations for blast fragmentation. J. Rock Mech. Geotech. Eng. 11, 1094–1109.
Ouchterlony, F., 2003. Influence of blasting on the size distribution and properties of muckpile fagments: a state-of-the-art review.
Ouchterlony, F., 2005b. What does the fragment size distribution of blasted rock look like? EFEE World Conference on Explosives and Blasting: 14/09/2005-16/09/2005. European Federation of Explosives Engineers, 189-199.
Paley, N., Kojovic, T., 2001. Adjusting blasting to increase SAG mill throughput at the Red Dog mine. proceedings of the annual conference on explosives and blasting technique. ISEE 1999, 65–82.
Parra, L.F.T., 2012. Study of blast-induced damage in rock with potential application to open pit and underground mines. University of Toronto (Canada).
Parra, H., Onederra, I., Michaux, S., Kuhar, L., Mcfarlane, A., Chapman, N., 2015. A study of the impact of blast induced conditioning on leaching performance. Miner. Eng. 74, 1–12.
Pawley, J., 2006. Handbook of biological confocal microscopy. Springer Science & Business Media.
Popov, O., Talovina, I., Lieberwirth, H., Duriagina, A., 2020. Quantitative microstructural analysis and X-ray computed tomography of ores and rocks—Comparison of results. Minerals 10, 129.
Pradhan, G.K., 1996. Explosives and Blasting Techniques, Mintech Publications.
Prasad, S., Choudhary, B., Mishra, A., 2017a. Effect of stemming to burden ratio and powder factor on blast induced rock fragmentation–a case study. IOP Conference Series: Materials Science and Engineering. IOP Publishing, 012191.
Prasad, S., Choudhary, B.S., Mishra, A.K., 2017b. Effect of Blast Design Parameters on Blast Induced Rock Fragmentation Size - A Case Study. Int. Conf. on Deep Excavation, Energy Resources and Production. IIT Kharagpur, India.
Rai, P., 2007. Modifications in the firing pattern, stemming column and bench stiffness for improved fragmentation in limestone quarry of the Philippines - a case study. IE (I) Journal-MN 88, 8.
Rai, P., 2021. A comparative investigation of inter-row delay timing vis-à-vis some rock properties on high sandstone benches. Indian J. Eng. Mater. Sci. (IJEMS) 27, 112–119.
Rai, P., Baghel, S., 2004. Investigation of firing patterns on fragmentation in an Indian opencast limestone mine. Quarry Manage. 31, 33–38.
Rai, P., Yang, H.S., 2010. Investigation of some blast design and evaluation parameters for fragmentation in limestone quarries. Tunnel Undergr. Space 20, 183–193.
Revnivtsev, V., 1988. We really need revolution in comminution. XVI International Mineral Processing Congress. Elsevier Science Publishers Amsterdam, pp. 93–114.
Rosin, P., 1933. Laws governing the fineness of powdered coal. J. Instit. Fuel 7, 29–36.
Roy, M., Paswan, R., Sarim, M., Kumar, S., Jha, R., Singh, P., 2016. Rock fragmentation by blasting-A review. J. Mines Met. Fuels 64, 424–431.
Ruan, Z., Li, M., Gao, K., Zhang, D., Huang, L., Xu, W., Liu, X., 2019. Effect of Particle Size Refinement on the Leaching Behavior of Mixed Rare-Earth Concentrate Using Hydrochloric Acid. ACS Omega 4 (6), 9813–9822.
Rustan, A., 1998. Rock Blasting Terms and Symbols: A Dictionary of Symbols and Terms in Rock Blasting and related areas like drilling, mining and rock mechanics. CRC Press.
Saharan, M., Mitri, H., Jethwa, J., 2006. Rock fracturing by explosive energy: review of state-of-the-art. Fragblast 10, 61–81.
Saliu, M., Akindoyeni, A., Okewale, I., 2013. Correlation between blast efficiency and uniaxial compressive strength. Int. J. Eng. Technol. 3, 799–805.
Sanchidrián, J.A., Segarra, P., López, L.M., Ouchterlony, F., Moser, P., 2009. Evaluation of some distribution functions for describing rock fragmentation data. Proc Fragblast 9, Proceedings of the ninth international symposium on rock fragmentation by blasting. Taylor & Francis Group, London, pp. 239–248.
Sanchidrián, J.A., Ouchterlony, F., Moser, P., Segarra, P., López, L.M., 2012. Performance of some distributions to describe rock fragmentation data. Int. J. Rock Mech. Min. Sci. 53, 18–31.
Sanchidrián, J.A., Ouchterlony, F., Segarra, P., Moser, P., 2014. Size distribution functions for rock fragments. Int. J. Rock Mech. Min. Sci. 71, 381–394.
Sassa, H., 1974. On the relation between the strength of a rock and the pattern of breakage by blasting. Adv. Rock Mech. 2, 1501–1505.
Scheffel, R., 2002. Copper heap leach design and practice. Mineral processing plant design, practice and control 2, 1571-1587.

Schlesinger, M., King, M., Sole, K., Davenport, W., 2011. Hydrometallurgical copper extraction. Extractive Metall. Copper 281–322.
Schuhmann Jr, R., 1940. Principles of comminution, I-size distribution and surface calculations. Am. Inst. Min. Met. Eng. Tech. Pub. 1189, 1–11.
Scott, A., 2009. Appendix 16—review of the impact of blasting on rock mass permeability. Bickham Coal WRA & Draft WMP, 43.
Seccatore, J., 2019. A review of the benefits for comminution circuits offered by rock blasting. REM-Int. Eng. J. 72, 141–146.
Seccatore, J., Origliasso, C., Tomi, G., 2013. Assessing a risk analysis methodology for rock blasting operations. Blasting in Mines-New Trends: Workshop Hosted by Fragblast.
Seo, Y., Jeong, G., Kim, J., Ichikawa, Y., 2002. Microscopic observation and contact stress analysis of granite under compression. Eng. Geol. 63, 259–275.
Sereshki, F., Hoseini, S., Ataei, M., 2016. Blast fragmentation analysis using image processing. Int. J. Min. Geo-Eng. 50, 211–218.
Shadabfar, M., Gokdemir, C., Zhou, M., Kordestani, H., Muho, E.V., 2020. Estimation of damage induced by single-hole rock blasting: A review on analytical, numerical, and experimental solutions. Energies 14, 29.
Shahrin, M., Abdullah, R., Sa'ari, R., Alel, M., Jeon, S., Jeon, B., 2019. Effect of burden to hole diameter ratio on rock fragmentation by blasting using LS-DYNA. ISRM Rock Dynamics Summit. OnePetro.
Shehu, S.A., Hashim, M.H.M., 2020. Evaluation of blast fragmentation and its benefits: a review of the paradigm and ambiguity. Int. J. Mini. Mineral Eng. 11, 338–358.
Shehu, S.A., Yusuf, K.O., Hashim, M., 2020. Comparative study of WipFrag image analysis and Kuz-Ram empirical model in granite aggregate quarry and their application for blast fragmentation rating. Geomech. Geoeng. 1–9.
Siddiqui, F.I., 2009. Measurement of size distribution of blasted rock using digital image processing. Eng. Sci. 20.
Sil'vestrov, V., 2004a. Application of the Gilvarry distribution to the statistical description of fragmentation of solids under dynamic loading. Combust., Explosion Shock Waves 40, 225–237.
Sil'vestrov, V., 2004b. Fragmentation of a Steel Sphere by a High-Velocity Impact on a Highly Porous Thin Bumper. Combust., Explosion Shock Waves 40, 238–252.
Singh, S.P., Cheung, D., 2017. Factors Governing the Muck Pile Characteristics. International Society of Explosives Engineers, Orlando, Florida, USA.
Singh, P., Roy, M., Paswan, R., Sarim, M., Kumar, S., Jha, R.R., 2016. Rock fragmentation control in opencast blasting. J. Rock Mech. Geotech. Eng. 8, 225–237.
Spanne, P., Thovert, J., Jacquin, C., Lindquist, W., Jones, K., Adler, P., 1994. Synchrotron computed microtomography of porous media: topology and transports. Phys. Rev. Lett. 73, 2001.
Sun, X.J., Sun, J.S., 2012. Research on the damage fracture of rock blasting based on velocity response spectrum. Appl. Mech. Mater. Trans Tech Publ, 1521-1527.
Sun, W., Zuo, Y., Wu, Z., Liu, H., Xi, S., Shui, Y., Wang, J., Liu, R., Lin, J., 2019. Fractal analysis of pores and the pore structure of the Lower Cambrian Niutitang shale in northern Guizhou province: Investigations using NMR, SEM and image analyses. Mar. Pet. Geol. 99, 416–428.
Thornton, D., Kanchibotla, S., Esterle, J.A., 2001. fragmentation model to estimate ROM size distribution of soft rock types. Proceedings of the Twenty-Seventh Annual Conference On Explosives and Blasting Technique, Vol I. International Society of Explosives Engineers, 41-53.
Tungol, Z., Kawamura, Y., Kitahara, I., Jang, H.D., 2019. Development of a Remote Rock Fragmentation Size Distribution Measurement System for Surface Mines Using 3D Photogrammetry. The 10th International Conference on Explosives and Blasting.
Vamshidhar, K., Venkatesh, H., 2010. Review of Models for Prediction of Rock Fragmentation due to Blasting. Journal of the Explosives Safety And Technology Society (Visfotak) India: Dealing With Safety And Technological Aspects Of The Explosives Industry 5, 23-30.
Van Geet, M., Swennen, R., Wevers, M., 2000. Quantitative analysis of reservoir rocks by microfocus X-ray computerised tomography. Sed. Geol. 132, 25–36.
Van Geet, M., Swennen, R., David, P., 2001. Quantitative coal characterisation by means of microfocus X-ray computer tomography, colour image analysis and back-scattered scanning electron microscopy. Int. J. Coal Geol. 46, 11–25.
Vesilind, P.A., 1980. The Rosin-Rammler particle size distribution. Resour. Recovery Conserv. 5, 275–277.
Vutukuri, V.S., Lama, R.D., Saluja, S., 1974. Handbook on mechanical properties of rocks.
Wang, G., Han, D., Qin, X., Liu, Z., Liu, J., 2020. A comprehensive method for studying pore structure and seepage characteristics of coal mass based on 3D CT reconstruction and NMR. Fuel 281, 118735.
Wang, Y., Uchida, T., Westferro, F., Rivers, M.L., Nishiyama, N., Gebhardt, J., Lesher, C. E., Sutton, S.R., 2005. High-pressure x-ray tomography microscope: Synchrotron computed microtomography at high pressure and temperature. Rev. Sci. Instrum. 76, 073709.
Wang, C., Zhu, Z.M., Zheng, T., 2012. The fracturing behavior of detected rock under blasting loads. Appl. Mech. Mater.. Trans Tech Publ 193–196.
Wei, X., Zhao, Z., Gu, J., 2009. Numerical simulations of rock mass damage induced by underground explosion. Int. J. Rock Mech. Min. Sci. 46, 1206–1213.
Wen, S., Hsih, C., Kuan, C., 1996. The application of a mineral exposure model in a gold leaching operation. Int. J. Miner. Process. 46, 215–230.
Wills, B.A., Finch, J., 2015. Wills' mineral processing technology: an introduction to the practical aspects of ore treatment and mineral recovery. Butterworth-heinemann.
Willson, C.S., Lu, N., Likos, W.J., 2012. Quantification of grain, pore, and fluid microstructure of unsaturated sand from X-ray computed tomography images.
Wong, T.F., 1985. Geometric probability approach to the characterization and analysis of microcracking in rocks. Mech. Mater. 4, 261–276.
Workman, L., Eloranta, J., 2003. The effects of blasting on crushing and grinding efficiency and energy consumption. In: Proc 29th Con Explosives and Blasting Techniques, Int Society of Explosive Engineers, Cleveland OH, 1-5.
Yang, R., Wang, Y., Ding, C., 2016. Laboratory study of wave propagation due to explosion in a jointed medium. Int. J. Rock Mech. Min. Sci. 81, 70–78.
Zhang, Z., 2008. Impact of rock blasting on mining engineering. Proceedings.
Zhang, Z., Luukkanen, S., 2021. Feasibility and necessity of mine to mill optimization in mining industry. Materia Medica 63–66.
Zhou, W.B., Li, K., Wang, Y.G., Zhang, L.J., Cheng, H.N., Zhou, H.B., 2019. Influence of particle size on copper recovery from sulfide ore by the moderately thermophilic microorganisms. Metall. Res. Technol. 116, 119.